DEVELOPING AND ANALYZING GREEN'S THEOREM METHODS TO SATISFY PREREQUISITES OF INVERSE SCATTERING SERIES MULTIPLE ATTENUATION FOR DIFFERENT TYPES OF MARINE ACQUISITION: TOWARDS EXTENDING PREREQUISITE SATISFACTION METHODS FOR ON-SHORE EXPLORATION

A Dissertation

Presented to

the Faculty of the Department of Physics

University of Houston

In Partial Fulfillment

of the Requirements for the Degree

Doctor of Philosophy

By

Lin Tang

August 2014

DEVELOPING AND ANALYZING GREEN'S THEOREM METHODS TO SATISFY PREREQUISITES OF INVERSE SCATTERING SERIES MULTIPLE ATTENUATION FOR DIFFERENT TYPES OF MARINE ACQUISITION: TOWARDS EXTENDING PREREQUISITE SATISFACTION METHODS FOR ON-SHORE EXPLORATION

Lin Tang

APPROVED:

Dr. Arthur B. Weglein, Chairman

Dr. Lawrence Pinsky

Dr. Lowell Wood

Dr. Donna Stokes

Dr. Mark Meier

Dean, College of Natural Sciences and Mathematics

ACKNOWLEDGMENTS

First, I would like to give my deepest gratitude to my thesis advisor, Dr. Arthur B. Weglein, for offering numerous guidance, encouragement and continuous support during my five years of graduate studies. I have always been amazed by his profound knowledge of physics, mathematics and geophysics, as well as his passion and enthusiasm for research and teaching. I will always benefit from what he taught me, not only the academic knowledge, but also his positive attitude towards life. Joining the group of Mission-Oriented Seismic Research Program has surely changed my life.

I would also like to thank my collaborators and colleagues in M-OSRP. Thanks to Dr. Paolo Terenghi for his invaluable instructions and guidance when I just started the program and knew nothing. Thanks to Dr. Jim Mayhan for his encouragement, help and detailed notes. Thanks to Dr. Fang Liu, Xu Li, Shih-Ying Hsu, Zhiqiang Wang for their generous support for my research. Special thanks to Hong Liang, Jinlong Yang, Di Chang, Chao Ma, Jing Wu, Xinglu Lin, Yanglei Zou and Jennifer Chin-Davis for sharing all the happiness and tears together for these years. I will treasure these memories for ever.

Thank you to my dissertation committee, Professor Lawrence Pinsky, Professor Lowell Wood, Professor Donna Stokes and Dr. Mark Meier, for their encouragement.

I thank my parents, Xiaoguang Tang and Hongyan Wang, for raising me, bearing with me, giving me unconditional love and trusting me no matter what I decided to do. You are the best parents. Thanks to my husband, Shohei Edamura, for all the love and understanding, and for bringing me to a brand new world.

DEVELOPING AND ANALYZING GREEN'S THEOREM METHODS TO SATISFY PREREQUISITES OF INVERSE SCATTERING SERIES MULTIPLE ATTENUATION FOR DIFFERENT TYPES OF MARINE ACQUISITION: TOWARDS EXTENDING PREREQUISITE SATISFACTION METHODS FOR ON-SHORE EXPLORATION

An Abstract of a Dissertation

Presented to

the Faculty of the Department of Physics

University of Houston

In Partial Fulfillment

of the Requirements for the Degree

Doctor of Philosophy

By

Lin Tang

August 2014

ABSTRACT

Inverse Scattering Series (ISS) algorithm can directly achieve the objectives of seismic processing without requiring any subsurface information. For achieving the potential capabilities of ISS algorithm, there are prerequisites that need to be satisfied. These prerequisites (including separating the reference wave from the reflected data, estimation of the source wavelet, and deghosting) can be satisfied by using Greens-theorem methods. This dissertation provides three contributions in satisfying the prerequisites for Inverse Scattering Series (ISS) multiple removal algorithm.

Chapter 2 examines the impact of a specific seismic-acquisition design (over/under cables) on the wave-separation methods. When the depth difference between the two cables is smaller, the wave-separation results are more accurate and have less errors. In the (x, ω) domain, Green's theorem requires the prediction point to be chosen away from the measurement cable, but it can accommodate a non-flat cable (e.g., at ocean bottom). Green's theorem in the (k, ω) domain can predict the separated wavefields on the cable. However, it requires a flat cable to perform Fourier transform over the measurement surface.

Chapter 3 presents a method for determining the correct reference velocities. The criteria for finding the correct reference velocities could be the invariances of source wavelet at different output points below the cable for the point source data, or the invariances along one radiation angle for the source array data.

The third project investigates and compares three different wavelet estimation methods, including: (1) the Wiener filter method, (2) the spectral division method, and (3) the Green's-theorem method. Comparing with the other two methods, the Green's-theorem method demonstrates strength when the data contains random noise, since it utilizes an integral along the measurement surface, which tends to reduce random noise.

CONTENTS

1. INTRODUCTION AND BACKGROUND

One of the objectives of seismic exploration is to extract the Earth's subsurface information from recorded seismic data in order to predict the location and extent of hydrocarbon accumulations. This dissertation is part of a comprehensive strategy to identify and address the outstanding and prioritized seismic-exploration challenges. Seismic-processing methods are effective and successful when their assumptions and prerequisites are satisfied. These methods can fail when the assumptions behind the processing methods are not satisfied. In many circumstances, the seismic processing and imaging methods require detailed and accurate subsurface information to be effective. However, as the petroleum industry world-wide trend moves to more complex and challenging offshore and on-shore plays, the inability to provide accurate and detailed subsurface information has become an increasingly serious impediment to the effectiveness of these methods. The inability of providing accurate and detailed subsurface information motivates the search for new innovative methods that can deliver more effective capabilities than the current mainstream methods. One way to address the challenge of the inability of providing detailed and accurate subsurface information is to develop new methods that do not need subsurface information.

Inverse Scattering Series (ISS) methods offer a direct way of achieving the objectives of seismic processing without requiring any subsurface information. Thus, it has the capability to address the pressing challenges of the current seismic exploration in the complex offshore and on-shore areas. However, while not requiring subsurface information, ISS methods have their own assumptions and requirements. The assumptions and requirements include having seismic data preprocessed before entering the comprehensive ISS algorithm. The prerequisites of ISS methods include: (1) identifying and separating the reference wave from the reflected data, (2) estimating the source signature and radiation pattern, and (3) source and receiver deghosting. When the prerequisites are satisfied successfully, ISS methods can deliver their potential capabilities and effectiveness in achieving the objectives of data processing. These prerequisites can be satisfied by using Green's-theorem methods. Green's-theorem methods for the prerequisites also do not require any subsurface information, thus are fully consistent with ISS methods. The combination of Green's theorem for wave separation and ISS methods provides every link in the processing chain with methods that are direct, and do not require subsurface properties as *a priori* information.

This thesis falls with the part of the comprehensive strategy that deals with several practical issues in the realization of prerequisites of ISS methods using the general Green's theorem methods. The greater realism and completeness we include in the math-physics description of the seismic experiment, the more effectiveness can be delivered by he seismic processing method.

Chapter 1 presents an introduction and background to the thesis. Section 1.1 provides a general introduction of seismic exploration and the data processing chain required by the ISS methods. Section 1.2 presents a tutorial on: (1) the basic theory of the inverse scattering series and (2) the Green's-theorem methods for satisfying the prerequisites of ISS methods. In the last section, an overview of the specific advances and contributions in this dissertation are reviewed, followed by a discussion of open issues and future plans.

1.1 Introduction

Seismic physics is a subject that uses physics and mathematics methods to analyze recorded seismic data, for predicting the structure and physical properties of the subsurface. One of the ultimate purposes is to explore for potential hydrocarbon reservoirs. Seismic surveys start with a man-made energy source generating a wave propagating down into the Earth. The energy source could be air-guns in marine seismic exploration, or dynamite, or Vibroseis for on-shore plays. As the wave propagates down, it meets significant changes in the subsurface properties, where a portion of the wave is reflected upward. The reflected waves are recorded by geophones or hydrophones on land or in the ocean, respectively. The collection of the recorded wavefields constitutes seismic reflection data. An example of the marine seismic acquisition is shown in Figure 1.1.

The character of seismic data is affected by the source that generates the wave, the properties of the Earth that the wave has experienced, and the nature of the measurement or recording device (Weglein and Stolt, 2014). Therefore, the data carries information from the energy source, the earth that the wave has experienced, and the recording device. For a given source, the seismic energy recorded by one receiver is a time sequence that contains several arrivals. These distinct arrivals are called seismic events. Events are separated by (relatively) quiet time intervals. From analyzing the reflected data (amplitude, phase, and shape), the subsurface properties can be predicted, and ultimately the objective is to estimate the location and properties of the potential hydrocarbon reservoirs in the Earth.

Many seismic processing and imaging methods require detailed and accurate subsurface information to process the data and image the subsurface. However, it becomes more and more difficult to provide the accurate and detailed subsurface information as the petroleum industry trend moves to more complex offshore and on-shore areas. New effective seismic processing methods are needed to address these challenges. The Inverse Scattering Series (ISS) provide the opportunity/potential to achieve all seismic processing goals without requiring any subsurface information. ISS methods have demonstrated great value and effectivenesses in providing capabilities (e.g., multiples prediction and removal, depth imaging and parameter inversion) for the seismic processing tool-box, without needing subsurface information (Weglein *et al.*, 2003; Weglein, 2013).

The steps that seismic data are taken through from the moment they are recorded until the time they are used to estimate subsurface properties can be described as a seismic processing chain. ISS methods require us to follow a specific processing chain to satisfy the data preparation requirement. At each processing step, we assume that the previous steps have been successfully achieved. In order to describe the processing chain, it is convenient to first define and catalogue different types of seismic events according to their history in the subsurface. After defining the groups of events, we describe the data processing chain required by ISS methods, for the final purpose of imaging and inversion of the subsurface properties.

First, I use a marine towed-streamer acquisition as an example to illustrate the event category (Figure 1.2). The events categories include:

(1) Reference wave. Perturbation theory separates the real world into two parts: the reference medium, whose property is known, plus a perturbation, which is the difference between the actual and reference properties. The wavefield that travels in the reference medium is defined as the reference wave P_0. The difference between the reference wave and the actual wave is the scattered wave P_s. The choice of reference

medium can be arbitrary depending on our purposes. The only commitment is the reference medium plus the perturbation give the actual Earth and experiment. In a marine environment, for the purpose of separating the reference wave and scattered wave, the reference medium is chosen as a half-space of water plus a half-space of air. In this reference medium, the reference wave includes the direct arrival, which travels directly from the source to the receiver, and its ghost, which starts the history from the source upward, hits the air-water interface, and then reaches the receiver. It is marked as Event 1 in Figure 1.2. The reference wave P_0 does not experience the subsurface in its history. Since the objective is to determine subsurface properties from the data, the first step in the seismic data processing is to remove P_0 from the scattered wave P_s. However, the reference wave contains information of the source wavelet, which is also an essential information required in many processing steps. Therefore, it is useful to identify and remove the reference wave before all the following data analysis.

(2) Ghosts. Ghosts include the source ghosts, the receiver ghosts, and the source-receiver ghosts (Event 3 and 4 in Figure 1.2). Source ghosts are the events that begin the propagation by traveling upward from the source to the air-water boundary, and receiver ghosts are the ones that end the history by traveling downward from the air-water boundary to the receiver. Source-receiver ghosts have both of the characters in their traveling history. The process of removing ghosts is called deghosting. Deghosting is an important data preprocessing step. Removing the ghosts will remove the notches in the frequency spectrum and boost the low frequency contents, thus it can enhance the resolution of seismic data.

After removing the reference wave and the ghosts from the data, seismic events are classified into two groups,

(3) Primaries. After removing the ghosts, we define the wavefields that have expe-

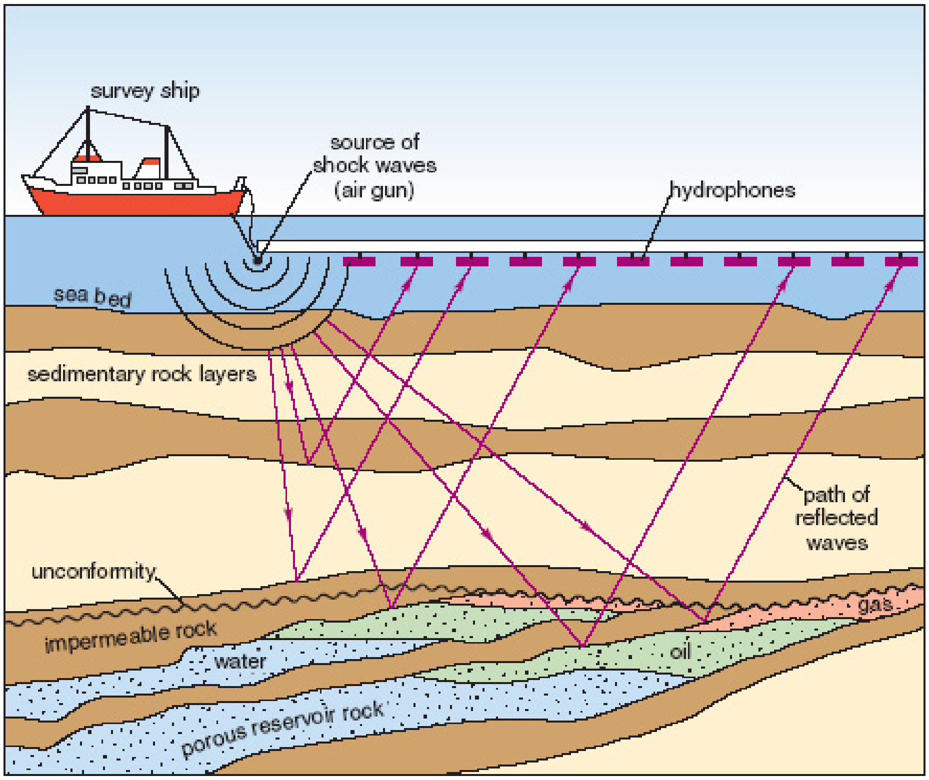

Fig. 1.1: *Marine seismic acquisition. (http://www.open.edu/openlearn/science-maths-technology/science/environmental-science/earths-physical-resources-petroleum/content-section-3.2.1)*

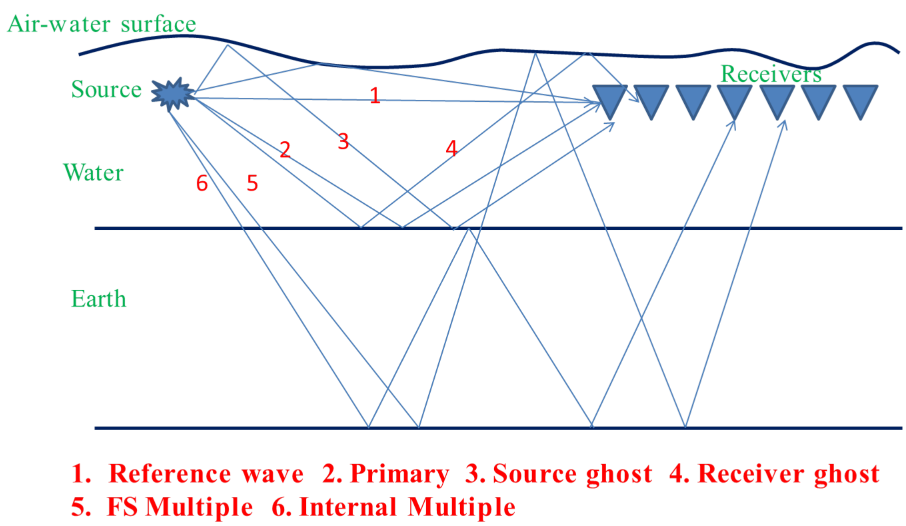

Fig. 1.2: *Seismic events and the category*

rienced only one upward reflection in the subsurface as the primaries (Event 2 in Figure 1.2).

(4) Multiples. After removing the ghosts, multiples are defined as the events that have been reflected multiple times in the subsurface. Depending on the location of the reflection, multiples can be classified as free surface multiples (Event 5 in Figure 1.2) and internal multiples (Event 6 in Figure 1.2). Free surface multiples are the events that have at least one downward reflection at the free surface (air-water or air-land boundary), whereas internal multiples have all their downward reflections happen below the free surface.

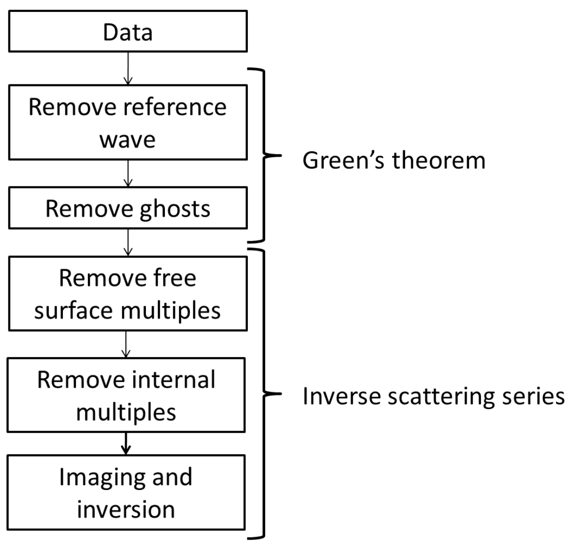

Fig. 1.3: *Seismic data processing chain*

Figure 1.3 shows the data processing chain required by ISS methods. After recording the data, we need to: (1) identify and remove the reference wave, (2) remove ghosts, (3) remove free surface multiples, (4) remove internal multiples, and finally (5) conduct imaging and inversion of subsurface. This processing chain can be understood starting from the objective of seismic exploration – extracting the subsurface information from the seismic data. Because the primaries have only experienced one upward reflection in the subsurface, it is relatively easy to estimate the structure and properties of reflectors from them. Currently, most seismic imaging and inversion methods have the primary-only assumption, which assumes that the seismic data contain only primaries.

Multiples contain information of the subsurface, too. However, the complex relationship between multiples and the subsurface reflectors makes it difficult or impossible to use multiples as useful signals for imaging. Therefore, we treat multiples as a form of coherence noise that need to be removed. Multiple removal is one of the biggest challenges in the seismic exploration. The current petroleum industry worldwide trend is moving towards areas with more complex and challenging offshore and on-shore plays. In these complex areas, multiples may be proximal to or interface with primaries, which will make the traditional adaptive-subtraction method fail. To solve this pressing issue, Inverse Scattering Series (ISS) methods provide a direct and comprehensive way to separate the multiples and the primaries. In particular, ISS free surface elimination method can predict the amplitude and phase of free surface multiples accurately, and ISS internal multiple attenuation algorithm can predict the exact phase and approximate amplitude of all internal multiples (Weglein *et al.*, 1997, 2003). It only uses reflected seismic data as the input, and does not require any subsurface information.

In order to deliver the effectiveness and power of ISS multiple removal algorithms, there are prerequisites that need to be satisfied. The prerequisites include: (1) identifying and separating the reference wave from the reflected data, (2) estimating the source signature and radiation pattern, and (3) source and receiver deghosting. These prerequisites can be realized by using Green's-theorem methods. Green's-theorem methods for the prerequisites also do not require any subsurface information, thus are fully consistent with ISS algorithms. The combination of Green's theorem for wave separation and ISS methods provides every link in the processing chain with methods that are direct, and do not require subsurface properties as *a priori* information.

In order to make ISS algorithms stronger, Mission-Oriented Seismic Research Program (M-OSRP) proposed a three-pronged strategy (Weglein, 2013), including:

(1) Improving satisfaction of prerequisites (in particular developing methods for on-shore);
(2) Building stronger algorithms (eliminating internal multiples of all orders);
(3) Developing consistent adaptive criteria and subsequent prediction methods.

The research in this dissertation falls in the comprehensive strategy in improving the satisfaction of data prerequisites of ISS multiple removal algorithm. In the next section, in order to understand why ISS methods and Green's-theorem methods can achieve all the processing objectives without subsurface information, a tutorial on the inverse scattering series and Green's-theorem methods for prerequisites will be given. For the details of the ISS multiple removal algorithm, readers are referred to Weglein *et al.* (2003), Weglein *et al.* (1997), Carvalho (1992) and Araújo (1994). Recent tests on offshore and on-shore field data can be found in Weglein (2013), Fu *et al.* (2010) and Ferreira (2011), and recent research towards multiple elimination can be found in Liang *et al.* (2013), Ma *et al.* (2011), Herrera and Weglein (2013) and Zou and Weglein (2013).

1.2 Inverse scattering series, Green's theorem, and seismic data preprocessing

In this section, a tutorial on the inverse scattering series and the Green's theorem methods for satisfying the data requirement of ISS methods will be given. Understanding the theory background of ISS methods will help us understand why this powerful algorithm can achieve all the seismic processing objectives in principle without needing any subsurface information.

Before introducing inverse-scattering series, we need to introduce the forward scattering series. Scattering theory separates the actual medium as the reference medium plus a perturbation. The choice of the reference medium can be arbitrary according to our purposes. The only requirement is the reference plus the perturbation give the actual earth and experiment. The forward scattering series construct the scattered wave from the knowledge of the reference medium and perturbation. In the actual medium, the wavefield satisfies the wave equation,

$$LG = \delta, \tag{1.1}$$

where L is the differential operator in the actual medium, G is the corresponding Green's function, and δ represents an impulsive source. Similarly, in the reference medium, the wave equation is,

$$L_0 G_0 = \delta, \tag{1.2}$$

where L_0 represents the differential operator of the reference medium, G_0 is the Green's function in the reference medium, and δ represents an impulsive source. We define the perturbation operator, V, and the scattered field ψ_s as the differences between the actual and the reference, e.g.,

$$V = L - L_0, \tag{1.3}$$

$$\psi_s = G - G_0. \tag{1.4}$$

In perturbation theory, Lippmann-Schwinger equation (Taylor, 1972) tells us,

$$G = G_0 + G_0 V G, \tag{1.5}$$

which shows the relationship of the actual wavefield G, the reference wavefield G_0, and the perturbation V. Now, if we substitute G on the right side of Equation 1.5 as itself, we can get an infinite series,

$$\begin{aligned} \psi_s = G - G_0 &= G_0 V G_0 + G_0 V G_0 V G_0 + ... && (1.6) \\ &= (\psi_s)_1 + (\psi_s)_2 + ... && (1.7) \end{aligned}$$

The above infinite series is the forward scattering series, which can predict the actual wavefield from the reference Green's function G_0 and the perturbation operator V. Forward scattering series is for modeling the wavefields from the known actual medium (known L_0 and V).

On the other hand, inverse scattering series help us to predict the perturbation from the measured data. Equation 1.7 indicates the scattered wavefield ψ_s can be written as a series in terms of the perturbation V. This suggests that the perturbation V can also be written as a series in terms of data,

$$V = V_1 + V_2 + V_3 + ..., \tag{1.8}$$

where V_i means the ith order in $(\psi_s)_{m.s.}$. If we substitute Equation 1.8 into Equation 1.6, and evaluate both sides of the equation on the measurement surface, we can get a series of equations by collecting the terms of equal order in the data,

$$
\begin{aligned}
(\psi_s)_{m.s.} = D &= (G_0 V_1 G_0)_{m.s.} && (1.9)\\
0 &= (G_0 V_2 G_0)_{m.s.} + (G_0 V_1 G_0 V_1 G_0)_{m.s.} && (1.10)\\
0 &= (G_0 V_3 G_0)_{m.s.} + (G_0 V_1 G_0 V_1 G_0 V_1 G_0)_{m.s.} \\
&\quad + (G_0 V_2 G_0 V_1 G_0)_{m.s.} + (G_0 V_1 G_0 V_2 G_0)_{m.s.} && (1.11)\\
&\vdots \quad .
\end{aligned}
$$

$(\psi_s)_{m.s.}$ is the measured scattered wavefield (the data), and G_0 can be calculated from the reference medium, hence, V_1 can be solved directly from Equation 1.9. V_1 is the linear portion of the perturbation in terms of the data. Having V_1, we can solve V_2 from Equation 1.10 similarly, and likewise for the further terms of V_i. In the end, the perturbation $V = V_1 + V_2 + V_3 + ...$ can be found directly from the scattered wavefield on the measurement surface and the reference medium information, without specifying any model type of the Earth (acoustic, elastic or anelastic etc.).

In fact, some subseries of the inverse scattering series can achieve some specific tasks on their own. In practice, we use the idea of “isolated-tasks” to isolate the purposes of data processing (Weglein *et al.*, 2003). Some particular subseries of inverse scattering series can predict and remove the free surface multiples, and some other subseries can accomplish the task of attenuating the internal multiples from the data. For the details of ISS multiple removal algorithm, readers are referred to Weglein *et al.* (2003), Weglein *et al.* (1997), Carvalho (1992) and Araújo (1994). Recent tests on offshore and on-shore field data can be found in Fu *et al.* (2010) and Ferreira (2011), and recent research towards beyond attenuation can be found in Liang *et al.* (2013), Ma *et al.* (2011), Herrera and Weglein (2013) and Zou and Weglein (2013).

To make the ISS algorithms achieve their high fidelity of multiple prediction, necessary prerequisites are needed. The prerequisites include: (1) removal of reference wave, (2) removal of ghosts, and (3) estimation of source signature and radiation patterns. Better delivery of the prerequisites will produce better multiple predictions. The Green's-theorem methods for prerequisites can achieve all these three goals without needing any subsurface information. The flexibility of Green's theorem comes from the freedom of the choice of reference medium in perturbation theory. For the current time, the Green's-theorem methods for P_0 P_s wave separation, deghosting, and wavelet estimation in the marine environment is mature and have already been tested in both synthetic data and field data (Zhang, 2007; Mayhan *et al.*, 2011; Mayhan and Weglein, 2013; Tang *et al.*, 2013; Yang *et al.*, 2013). In this section I will use the marine seismic exploration as an example to introduce the basic theory of Green's-theorem-derived seismic data preprocessing methods.

Let's assume that a source $A(t)$ is placed at $\vec{r_s}$, and a receiver is placed at $\vec{r}$. In an acoustic, constant density world, the pressure wavefield P satisfies the wave equation,

$$\left(\nabla^2 - \frac{1}{c^2(\vec{r})}\frac{\partial^2}{\partial t^2}\right) P(\vec{r}, \vec{r}_s, \omega) = A(t)\delta(\vec{r} - \vec{r_s}). \tag{1.12}$$

Fourier transform over time t gives the equation in the frequency domain,

$$\left(\nabla^2 + \frac{\omega^2}{c^2(\vec{r})}\right) P(\vec{r}, \vec{r}_s, \omega) = A(\omega)\delta(\vec{r} - \vec{r_s}). \tag{1.13}$$

Perturbation theory separates the actual medium into a combination of an unperturbed medium, called the reference medium, and a perturbation. Perturbation α is defined by

$$\frac{1}{c^2(\vec{r})} = \frac{1}{c_0^2}[1 - \alpha(\vec{r})],$$

where c_0 is the velocity in a homogeneous reference medium. Now the actual velocity is described in terms of the reference velocity, c_0, and a perturbation, $\alpha(\vec{r})$. Then Equation 1.13 becomes

$$\left(\nabla^2 + \frac{\omega^2}{c_0^2}\right) P(\vec{r}, \vec{r}_s, \omega) = \underbrace{\frac{\omega^2}{c_0^2}\alpha(\vec{r})P(\vec{r}, \vec{r}_s, \omega) + A(\omega)\delta(\vec{r} - \vec{r}_s)}_{\rho(\vec{r},\omega)}. \tag{1.14}$$

The right-hand side of Equation 1.14 can be viewed as the source ρ of the wavefield P. The source ρ has two terms: the perturbation α, which generates the scattered wave P_s, and the active source $A(\omega)$, which is the energy source that generates the wave P. The corresponding Green's function satisfies,

$$\left(\nabla^2 + \frac{\omega^2}{c_0^2}\right) G_0(\vec{r}, \vec{r'}, \omega) = \delta(\vec{r} - \vec{r'}). \tag{1.15}$$

Equation 1.15 has infinite number of solutions of Green's functions. Among these infinite number of solutions, the causal solution, G_0^+, is generated when the source goes off and moves away from the source. On the other hand, the anti-causal solution, G_0^-, exists for the time before the source explodes, and moves towards the source. In order to predict a physical wavefield P, we need to use the causal solution G_0^+ to calculate, *i.e.*,

$$\begin{aligned} P(\vec{r}, \vec{r_s}, \omega) &= \int_\infty G_0^+(\vec{r}, \vec{r'}, \omega)\rho(\vec{r'}, \omega)d\vec{r'} \qquad (1.16) \\ &= \int_\infty G_0^+(\vec{r}, \vec{r'}, \omega)\left[k^2\alpha(\vec{r'})P(\vec{r'}, \vec{r_s}, \omega) + A(\omega)\delta(\vec{r'} - \vec{r_s})\right]d\vec{r'} \\ &= \int_\infty G_0^+(\vec{r}, \vec{r'}, \omega)k^2\alpha(\vec{r'})P(\vec{r'}, \vec{r_s}, \omega)d\vec{r'} + A(\omega)G_0^+(\vec{r}, \vec{r_s}, \omega), \qquad (1.17) \end{aligned}$$

where $k = \omega/c_0$. The first term on the right-hand side of Equation 1.17 is the source that generates the difference between the total wavefield P and the reference wavefield P_0. Therefore, P_0 is given by,

$$P_0(\vec{r}, \vec{r_s}, \omega) = A(\omega)G_0^+(\vec{r}, \vec{r_s}, \omega). \qquad (1.18)$$

The difference between P and P_0 is defined as the scattered wavefield P_s, which is

$$P_s = P - P_0. \qquad (1.19)$$

Thus, P_s satisfies

$$P_s(\vec{r}, \vec{r_s}, \omega) = \int_\infty G_0^+(\vec{r}, \vec{r'}, \omega)\frac{\omega^2}{c_0^2}\alpha(\vec{r'})P(\vec{r'}, \vec{r_s}, \omega)d\vec{r'}. \qquad (1.20)$$

On the other hand, according to Green's theorem, a vector field $\mathbf{A}$ satisfies relationship,

$$\int_V d\vec{r'}(\nabla \cdot \mathbf{A}) = \oint_S dS\hat{n} \cdot \mathbf{A}. \qquad (1.21)$$

Now assuming the field has a form $\mathbf{A} = \phi\nabla\psi - \psi\nabla\phi$, where ϕ and ψ are scalar fields, then we have the Green's second identity,

$$\int_V (\phi \nabla'^2 \psi - \psi \nabla'^2 \phi) d\vec{r'} = \oint_S [\phi \nabla' \psi - \psi \nabla' \phi] \cdot \hat{n} dS. \tag{1.22}$$

Now suppose that $\phi = P$ and $\psi = G_0$. Plugging Equation 1.14 and Equation 1.15 into Equation 1.22, we have the left hand side of Equation 1.22,

$$\begin{aligned} LHS &= \int_V (P \nabla'^2 G_0 - G_0 \nabla'^2 P) d\vec{r'} \\ &= \int_V \Bigg(P(\vec{r'}, \vec{r_s}, \omega) \left[-\frac{\omega^2}{c_0^2} G_0(\vec{r}, \vec{r'}, \omega) + \delta(\vec{r} - \vec{r'}) \right] \\ &\quad - G_0(\vec{r}, \vec{r'}, \omega) \left[-\frac{\omega^2}{c_0^2} P(\vec{r'}, \vec{r_s}, \omega) + \rho(\vec{r'}, \omega) \right] \Bigg) d\vec{r'} \\ &= \int_V P(\vec{r'}, \vec{r_s}, \omega) \delta(\vec{r} - \vec{r'}) d\vec{r'} - \int_V G_0(\vec{r}, \vec{r'}, \omega) \rho(\vec{r'}, \omega) d\vec{r'}. \end{aligned} \tag{1.23}$$

The right hand side of Equation 1.22 is the surface integral,

$$RHS = \oint_S [P(\vec{r'}, \omega) \nabla' G_0(\vec{r}, \vec{r'}, \omega) - G_0(\vec{r}, \vec{r}', \omega) \nabla' P(\vec{r'}, \omega)] \cdot \hat{n} dS.$$

The value of the first term on the left hand side of Equation 1.22 depends on where the observation point $\vec{r}$ is. If $\vec{r}$ is chosen to be inside the volume V, then the first term becomes $P(\vec{r}, \vec{r_s}, \omega)$, due to the character of Dirac delta function. When $\vec{r}$ is outside of the volume V, the volume integral becomes zero. Therefore,

$$\left.\begin{array}{cc} \vec{r}\ \ in\ \ V & P(\vec{r}, \omega) \\ \vec{r}\ \ out\ \ V & 0 \end{array}\right\} = \int_V G_0(\vec{r}, \vec{r'}, \omega) \rho(\vec{r'}, \omega) d\vec{r'} + \oint_S [P(\vec{r'}, \omega) \nabla' G_0(\vec{r}, \vec{r'}, \omega) - G_0(\vec{r}, \vec{r'}, \omega) \nabla' P(\vec{r'}, \omega)] \cdot \hat{n} dS. \tag{1.24}$$

Equation 1.24 provides the basis for several applications of Green's theorem in seismic data processing. It enables us to predict the wavefield inside a volume V, when we have the surface measurements of the wavefields and a complete knowledge of the medium inside the volume, including the active sources and the medium properties. All the Green's-theorem-based seismic data preprocessing methods in this dissertation, including separating the reference wave P_0 and scattered wave P_s, source wavelet and radiation estimation, and deghosting, use the form of Equation 1.24 as a framework and a starting point.

When deriving Equation 1.24, the only requirement of Green's function is that it satisfies Equation 1.15. This means G_0 can be either causal, or anti-causal, or any combinations of them, as long as it satisfies Equation 1.15. When we choose $G_0 = G_0^+$, and $\vec{r}$ to be inside V, we can compare Equation 1.24 with Equation 1.16. Equation 1.16 can be rewritten as,

$$P(\vec{r}, \vec{r_s}, \omega) = \int_{\infty} G_0^+ \rho d\vec{r'} = \int_V G_0^+ \rho d\vec{r'} + \int_{\infty - V} G_0^+ \rho d\vec{r'}. \tag{1.25}$$

Equation 1.25 is valid at any point $\vec{r}$ in the space, while Equation 1.24 can only provide the wavefield P inside the volume V. If we use G_0^+ in Equation 1.24, and choose the observation point $\vec{r}$ inside the volume V, the wavefield predicted by both equations should be equal. The first term in both equations are the same. Therefore, the second term should be equal, *i.e.*,

$$\int_{\infty - V} G_0^+ \rho d\vec{r'} = \oint_S [P \nabla G_0^+ - G_0^+ \nabla P] \cdot \hat{n} dS. \tag{1.26}$$

The above equation shows that the surface integral gives the contribution to the portion of the field inside the volume V due to the sources outside the volume (Morse and Feshbach, 1953). The surface integral extinguishes the portion of the field in the volume due to the sources inside the volume. This property can be used to separate the fields into two parts: the fields that are contributed by the sources inside the volume, and the fields that are due to the sources outside the volume. In this dissertation, in each chapter I will start from the basis of Green's theorem to discuss the specific form of Green's theorem for achieving our purposes (wavefield separation, wavelet estimation, *etc.*).

1.3 Overview of the dissertation

This dissertation focuses the discussion in several outstanding issues in the realization of the theories for satisfying prerequisites of ISS methods, including: (1) how the actual data acquisition would impact the wave separation in the marine environment, (2) how can we determine the reference velocities for land application, and (3) how can we choose the appropriate wavelet estimation methods for different purposes. The more realism and completeness we include in the description of the seismic experiment, the more effectiveness these theories can deliver.

Chapter 2 discusses several practical issues of separating the reference wave and the scattered wave in the marine seismic exploration. A realistic and accurate description of how data are actually acquired is analyzed and incorporated. Green's theorem requires the wavefield P and its normal derivatives P_n on the measurement surface as the input. In the marine application, over/under cable is often used for acquiring the data, which measures the pressure wavefield at different depths. I use a finite-difference approximation to obtain the normal derivatives of the wavefield. The test result shows that the closer of the over/under cable is, the less error will be predicted in the wave-separation results. An adjustment of the current theory is proposed for avoiding the finite difference approximation. In addition, the Green's theorem wave separation method is studied both in the (x, ω) domain and in the (k, ω) domain. In the (x, ω) domain, Green's theorem requires the prediction point of the separated wave to be chosen away from the measurement cable. But it can accommodate a non-flat cable, which is often used at ocean bottom. On the other hand, Green's theorem in the (k, ω) domain can predict the wavefield of P_0 or P_s on the cable (separating the wave types in the measured data). However, it requires a flat cable to perform Fourier transform over the measurement surface.

In Chapter 3, I describe and address an issue that arises with the extension of the marine prerequisites satisfaction to land application. In theory, the reference medium information is supposed to be known. For the on-shore application, the near surface medium property is often difficult to determine. ISS methods require the reference medium to agree with the actual medium at and above the measurement surface. Therefore, finding the reference medium property becomes a challenge for land. Chapter 3 presents a method for determining the correct reference velocities. The method depends on the fact that the wave-separation methods to determine the reference wave and the source signature will produce the same wavelet at every output point below the cable when the reference medium is correct. By "correct" we mean the reference medium agrees with the actual medium at and above the measurement surface. I propose to use the invariances of source wavelet at different output points below the cable (for the point source data), or invariances in one radiation angle (for the source array data), as the criteria for having the correct reference velocities. This idea is first shown using an analytic example and then tested using a synthetic example in the marine environment. Future study will move towards complex on-shore near surface medium and reference wave prediction, based on a similar thinking of using the invariances as the criteria.

Chapter 4 starts to discuss several different methods for source wavelet estimation, including: (1) the Wiener filter method, (2) the spectral division method, and (3) the Green's theorem method. The comparison will help us choose the appropriate method for wavelet estimation under different circumstances and purposes. The Wiener filter method and spectral division method offer a direct way of extracting wavelet from the reference wave. However, the reference wave may not always be available from the data directly. The Green's theorem method demonstrates strength when the data contains noise, since it utilizes an integral along the measurement surface, which tends to reduce random noise. In Chapter 4, I also present the wavelet estimation result from a marine field data set, using the Wiener filter method. The wavelet result is used in the first ISS depth imaging field data test for the purpose of data regularization.

Chapter 5 gives a summary of this dissertation.

2. IMPACT OF DATA ACQUISITION ON THE WAVE SEPARATION METHOD

2.1 Chapter overview

In this chapter, I discuss several practical issues when realizing the Green's-theorem-based wave-separation theory in the marine seismic exploration. A realistic and accurate description of how data are actually acquired is analyzed and incorporated for a better realization of the wave separation theories. I consider how the details and specifics of seismic acquisition impact the P_0 P_s wave separation theories, as well as how can we best accommodate the reality of the data acquisition design for the realization of Green's theorem. Green's-theorem methods can separate P_0 and P_s through a surface integral along the cable, without requiring any subsurface information. The inputs of Green's theorem are the wavefield P and its normal derivative P_n on the measurement surface. However, in the marine application, either over/under cable, which measures the pressure wavefields at different depths, or the dual sensor cable, which measures both the pressure and the vertical velocities, are used for acquiring the data. To obtain the normal derivatives of the wavefield, I use a finite-difference approximation of the wavefields from the over/under cable. Test results show that this approximation will generate some errors when the depth between the over/under cable is large. This issue can be solved by constructing the wavefield and its normal derivative at a new depth between the over/under cable, using the measured wavefields on both cables and a Green's function that vanishes at the two cables. This is an adjustment of the wave separation theory, for better accommodating the way data are actually acquired.

In addition, the wave-separation theory is studied both in the (x, ω) domain and in the (k, ω) domain. In the (x, ω) domain, Green's theorem requires that the depth difference between the prediction point and the measurement surface need to be at least half of the receiver sampling. But it can accommodate a non-flat cable (e.g., at ocean bottom). In order to predict the wavefield of P_0 or P_s on the cable (separating the wave types in the measured data), Green's theorem in the (k, ω) domain can achieve it. However, it requires a flat measuring cable to perform Fourier transform over the measurement surface.

2.2 Theory

In Section 1.2, I have discussed the general framework of Green's theorem for its applications in the seismic data preprocessing. Now I will focus on the application for separating the reference wave P_0 and the scattered wave P_s, using the marine exploration as an example.

The freedom of choosing the reference medium is the key of the flexibility and power of Green's-theorem methods. The only assumption is that the reference medium plus the "sources" give the actual medium and experiment. The inverse-scattering series methods require that the reference medium agree with the actual medium at and above the measurement surface. Therefore, in the marine environment, we can choose the reference medium as a half-space of air plus a half-space of water, separated by a free surface (Figure 2.1). Then on top of this reference mdium, there are two sources: the air guns in the water column and the earth below the ocean bottom (Figure 2.2). In this reference medium, the Green's function G_0 has two parts: G_0^d, which travels directly from the source to the receiver, and G_0^{FS}, which has a downward reflection at the free surface (Figure 2.3).

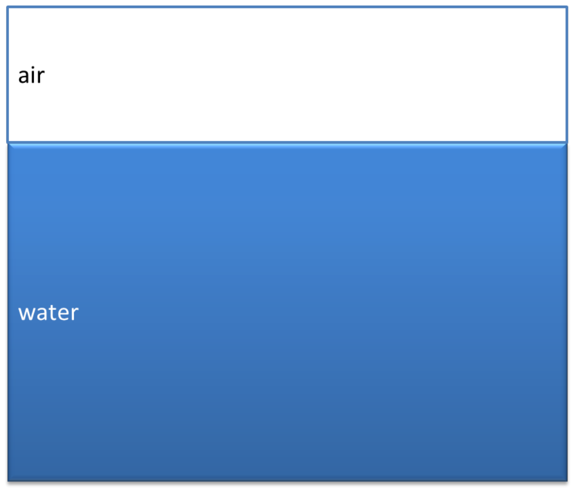

Fig. 2.1: *Choosing the reference medium as a half-space of air and a half-space of water in marine exploration*

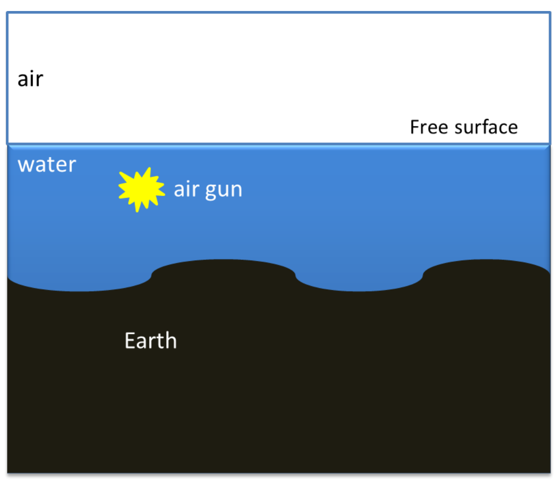

Fig. 2.2: *Two sources: air guns and earth*

Equation 1.26 tells us that the surface integral of $\oint_S [P\nabla G_0^+ - G_0^+ \nabla P] \cdot \hat{n} dS$ gives the contribution to the field inside the volume V due to the sources outside the volume, when evaluated at $\vec{r}$ inside V. Choosing the reference medium as shown in Figure 2.1, and the volume V as shown in Figure 2.4, when $\vec{r}$ is inside V, the above surface integral provides the portion of wavefield P due to the sources outside the volume, which are the active sources in this picture. The portion contributed by the active sources are the reference wavefield P_0, which is,

$$\begin{aligned} P_0(\vec{r},\omega) &= \int_{\infty - V} d\vec{r'} \rho_{airguns}(\vec{r'},\omega) G_0^+ \\ &= \oint_S [P \nabla G_0^+ - G_0^+ \nabla P] \cdot \hat{n} dS. \end{aligned} \tag{2.1}$$

Equation 2.1 can provide the reference wavefield P_0 at any point $\vec{r}$ below the measurement surface, as long as we have P and $\frac{\partial P}{\partial n}$ on the measurement surface. The active source can be a single point source, or a source array, or with any character. It also does not need the information of the subsurface. This character of Green's theorem is fully consistent with the Inverse Scattering Series methods, thus can serve it perfectly.

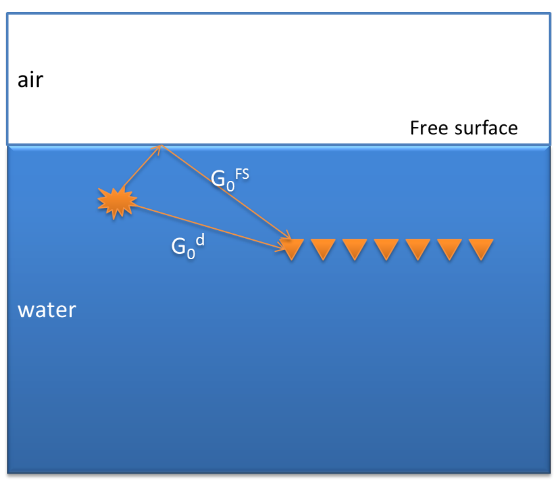

Fig. 2.3: *Green's function in the reference medium*

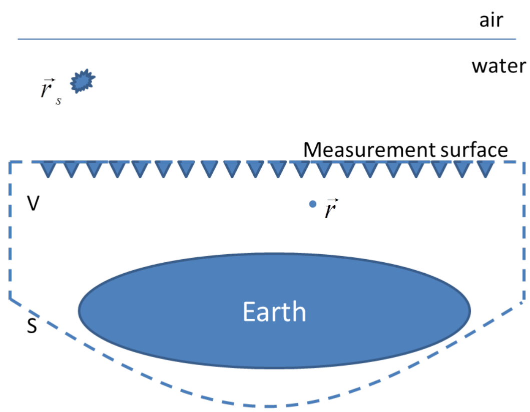

Fig. 2.4: *Choosing V as the hemisphere infinite space below the cable, and $\vec{r}$ below the cable to predict P_0.*

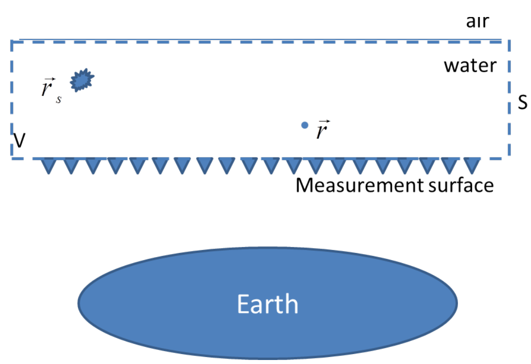

Fig. 2.5: *Choosing V as the space between the free surface and the cable, and $\vec{r}$ above the cable to predict P_s.*

Similarly, for the purpose of predicting the scattered wave P_s, we can choose the volume as the region between the free surface and the measurement surface, with the prediction point inside the volume (Figure 2.5). Then outside the volume the only source is the Earth. The wavefield that is contributed from the earth is the scattered wave P_s. Therefore, when we choose the volume as in Figure 2.5 and $\vec{r}$ inside V, we can have,

$$P_s(\vec{r}, \omega) = \oint_S [P\nabla G_0^+ - G_0^+ \nabla P] \cdot \hat{n} dS. \tag{2.2}$$

Again, Equation 2.2 provides the portion of scattered wave P_s at any point above the measurement surface from the wavefield P and its derivative $\frac{\partial P}{\partial n}$ on the measurement surface.

The surface integral along the closed surface S in practice becomes the integral along the measurement surface. For the case of choosing V as the lower half semi-hemisphere (Figure 2.4), the contribution from the infinite far-away boundary vanishes when $|\vec{r}| \to \infty$ when using a causal Green's function G_0^+. From Equation 1.24, when $\vec{r}$ is inside V,

$$\begin{aligned} P(\vec{r},\omega) &= \int_V G_0(\vec{r},\vec{r'},\omega)\rho(\vec{r'},\omega)d\vec{r'} \\ &+ \oint_S [P(\vec{r'},\omega)\nabla' G_0(\vec{r},\vec{r'},\omega) - G_0(\vec{r},\vec{r'},\omega)\nabla' P(\vec{r'},\omega)] \cdot \hat{n} dS. \end{aligned} \quad (2.3)$$

As $|\vec{r}| \to \infty$, the second term of Equation 2.3 must vanish if $G_0 = G_0^+$, because

$$P(\vec{r},\omega) = \int_\infty G_0^+(\vec{r},\vec{r'},\omega)\rho(\vec{r'},\omega)d\vec{r'}. \quad (2.4)$$

This condition only holds when using a causal Green's function. If using an anti-causal Green's function G_0^-, the surface integral does not vanish at a large $|\vec{r}|$.

For the volume chosen as in Figure 2.5, the contribution from the free surface also vanishes, because both P and G_0 are zero at this surface. Therefore, the integral happens only along the measurement surface.

2.3 Impact of acquisition on the wave separation result

From Equation 2.1 and 2.2, we can see that the inputs of Green's theorem for wave separation are the wavefield P and its normal derivative $\frac{\partial P}{\partial n}$ on the measurement surface. However, in practice, data acquisition can often affect the wave separation results. In the marine environment, both over/under towed streamers and dual-sensor streamers are recently widely used in the industry (Moldoveanu *et al.*, 2007; Carlson *et al.*, 2007). An over/under towed-streamer consists of two streamers at different depth (over/under) in the same vertical plane. Both of these cables measure the pressure wavefield P using hydrophones. On the other hand, a dual sensor streamer is one cable with sensors that can measure the pressure wavefield, P, and the vertical component of the particle velocity, V_z, at the same depth simultaneously. Both over/under cable and dual sensor cable have their advantages and shortcomings. For the over/under cable, the instrument responses from both cables are the same, but the measured fields are at different depths. Dual sensor cable can measure P and V_z at the same depth, but the measurement of P and V_z have instrument response differences. In addition, the measurement of V_z can have issues at the low frequency. For the Green's theorem-based deghosting method, Weglein *et al.* (2013) derived the industry standard $P - V_Z$ summation deghosting method from Green's theorem in the (k, ω) domain. Weglein *et al.* (2013) proposed a new deghosting method that can avoid the issues both in the (x, ω) domain and the $P - V_z$ issues. In this chapter, I only discuss the impact of over/under streamer acquisition to the Green's theorem-based P_0 P_s wave separation results.

2.3.1 The depth difference between the over/under cable

Since the wavefield P is the recorded data, the normal derivative P_n needs to be calculated from the measurement of wavefield P in the marine environment. When using an over/under cable, an easy way to calculate the normal derivative is to use a finite approximation, which means subtracting the data of the upper cable from the data of the lower cable and then divide by their depth difference, *i.e.*,

$$\frac{dP(\frac{z_2-z_1}{2})}{dz} = \frac{P(z_2) - P(z_1)}{z_2 - z_1}. \tag{2.5}$$

As the above equation shows, the normal derivative of P is at the depth $(z_2 - z_1)/2$, rather than at z_1 or z_2, where wavefield P is measured. Inputting $dP(\frac{z_2-z_1}{2})/dz$ and $P(z_1)$ or $P(z_2)$ into the form of Green's theorem, the finite approximation will cause some errors in the wave separation results.

In our synthetic tests using the reflectivity method, we first used a 1D acoustic model with the source at 5 m and two cables, one at a depth of 45 m and one at 50 m. (The cables were placed unrealistically deep to better illustrate the results.) Thus the two cables are separated by 5 m. An example of the total wavefield at depth 50 m is shown in Figure 2.6.

Using Green's theorem, the scattered wave P_s is predicted at 20 m, and P_0 is predicted at 80 m, as shown in Figure 2.7. Next, I reduce the depth difference between the two cables to 1 m (one cable at 49 m, the other at 50 m). With the new configuration, the predicted P_s at 20 m and P_0 at 80 m are shown in Figure 2.8.

From these two results, it can be seen that when the depth difference is 5 m (in Figure 2.7), there are several errors in both cases of P_0 and P_s prediction, whereas

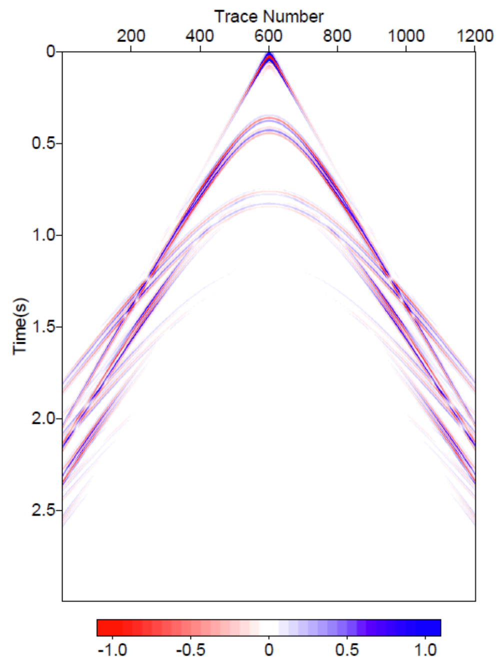

Fig. 2.6: *Synthetic data constructed at depth $z = 50$ m using reflectivity method*

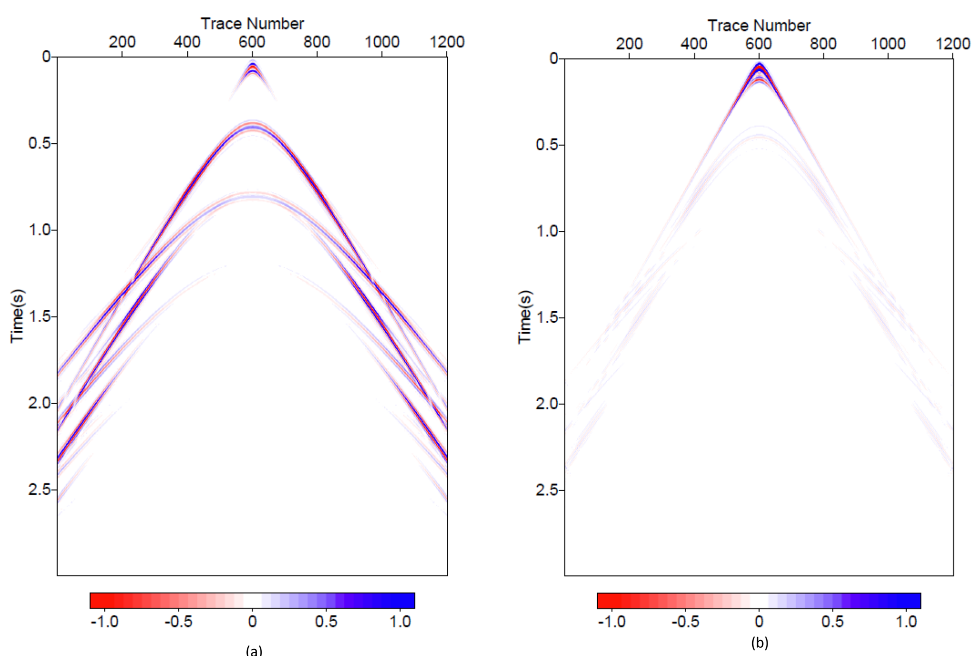

Fig. 2.7: *Using an over/under cable with a 5 m depth difference. (a) P_s predicted at 20 m, (b) P_0 predicted at 80 m.*

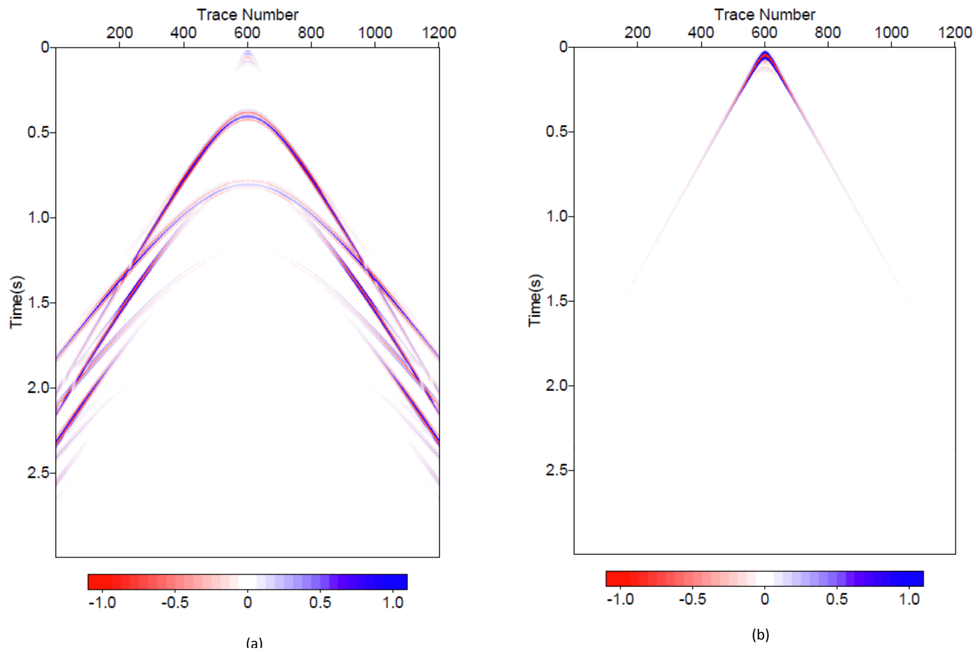

Fig. 2.8: *Using an over/under cable with a 1 m depth difference. (a) P_s predicted at 20 m, (b) P_0 predicted at 80 m.*

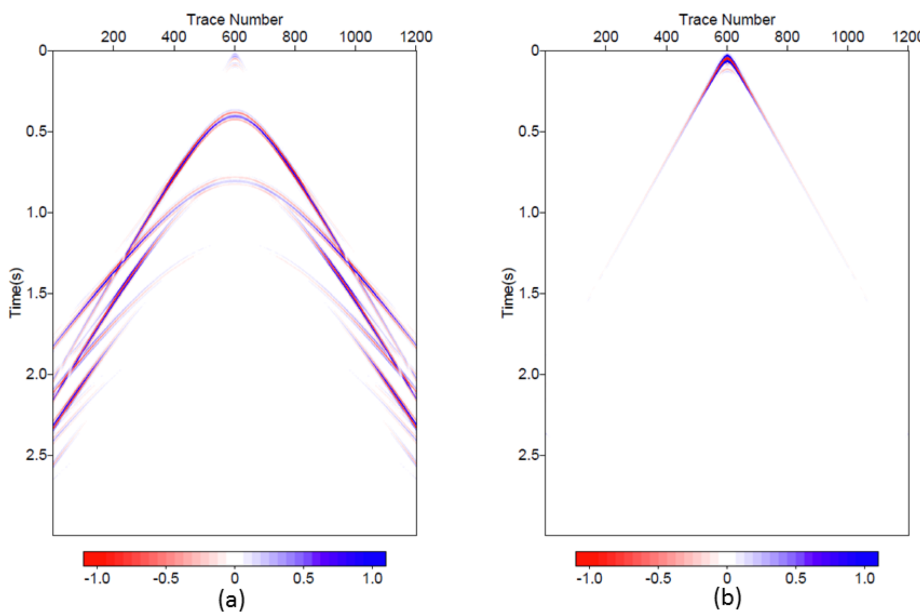

Fig. 2.9: *Using three cables. (a) P_s predicted at 20 m, (b) P_0 predicted at 80 m.*

in Figure 2.8, the predicted results are very satisfying. This indicates that reducing the difference in the cable depths can significantly increase the accuracy of wave separation results.

In reality, it is hard to make the over/under cable very close, as there are mechanic issues (e.g., two cables might tangle together). To obtain an accurate dP/dz at the same depth of P, now I consider the acquisition that uses three cables at different depth. If assuming that the three cables are placed with equal vertical distance (depth 45 m, 50 m and 55 m in the example), then dP/dz at depth 50 m can be calculated by

$$\frac{dP}{dz}(50) = \frac{P(55) - P(45)}{55 - 45}.$$

So now we have both P and dP/dz at depth 50 m. Using them as the inputs of Green's theorem, the predicted P_s at depth 20 m and P_0 at 80 m are shown in Figure 2.9. Comparing with the previous result from two cables separated by 5 m as shown in Figure 2.7, it is clearly that the errors in the three cables case are less than those in the result of two cables.

Another method that can avoid the issue of finite approximation of P_n is to construct the wavefield P and P_n at a new depth between the upper and the lower cable, using Green's theorem. Now choose the volume as the space between the two cables, and purposely construct the Green's function that vanishes on both the two cables, defined as G_0^{DD}. With this new Green's function G_0^{DD}, the second term in the integral will vanish on the surface. Therefore, the new wavefield P can be calculated from

$$P(\vec{r}, \omega) = \oint_S P(\vec{r'}, \omega) \frac{dG_0^{DD}(\vec{r}, \vec{r'} m\omega)}{dz'} d\vec{r'}. \tag{2.6}$$

Because there is no "source" ρ in this volume. A derivation of Equation 2.6 gives P_n,

$$\frac{dP(\vec{r},\omega)}{dz} = \oint_S P(\vec{r'},\omega)\frac{d^2G_0^{DD}(\vec{r},\vec{r'}m\omega)}{dz'^2}d\vec{r'}. \tag{2.7}$$

The calculation of G_0^{DD} is shown in Appendix A, which is enlightened from Zhang (2007). Now having P and P_n at the new depth between the over/under cable, it is possible to input them into Green's theorem method for wave separation, without using any finite difference approximation.

2.3.2 The depth of the predicted wave

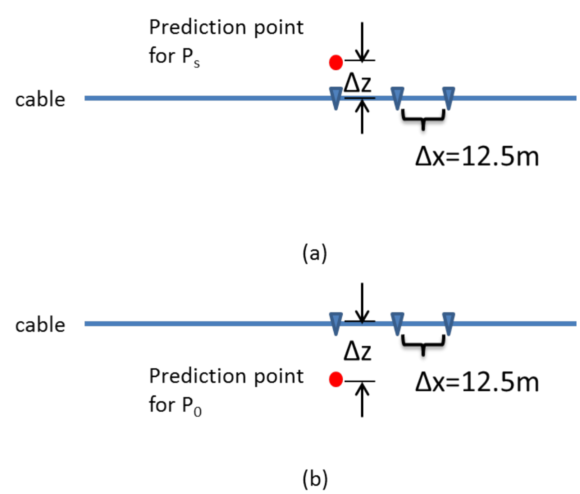

Fig. 2.10: *The definition of $\triangle z$ for predicting (a) P_s (b) P_0.*

Other factors may affect the estimated results. The actual experiment shows that the choice of the prediction depth can change the quality of the wave separation result. The depth difference between the prediction point and the measurement surface is defined as $\triangle z$, illustrated in Figure 2.10. The sampling interval between the receivers is defined as $\triangle x$, which can be used as a unit to measure the length of $\triangle z$. Figure 2.11 shows four results of P_s predicted at different depths above the measurement surface.

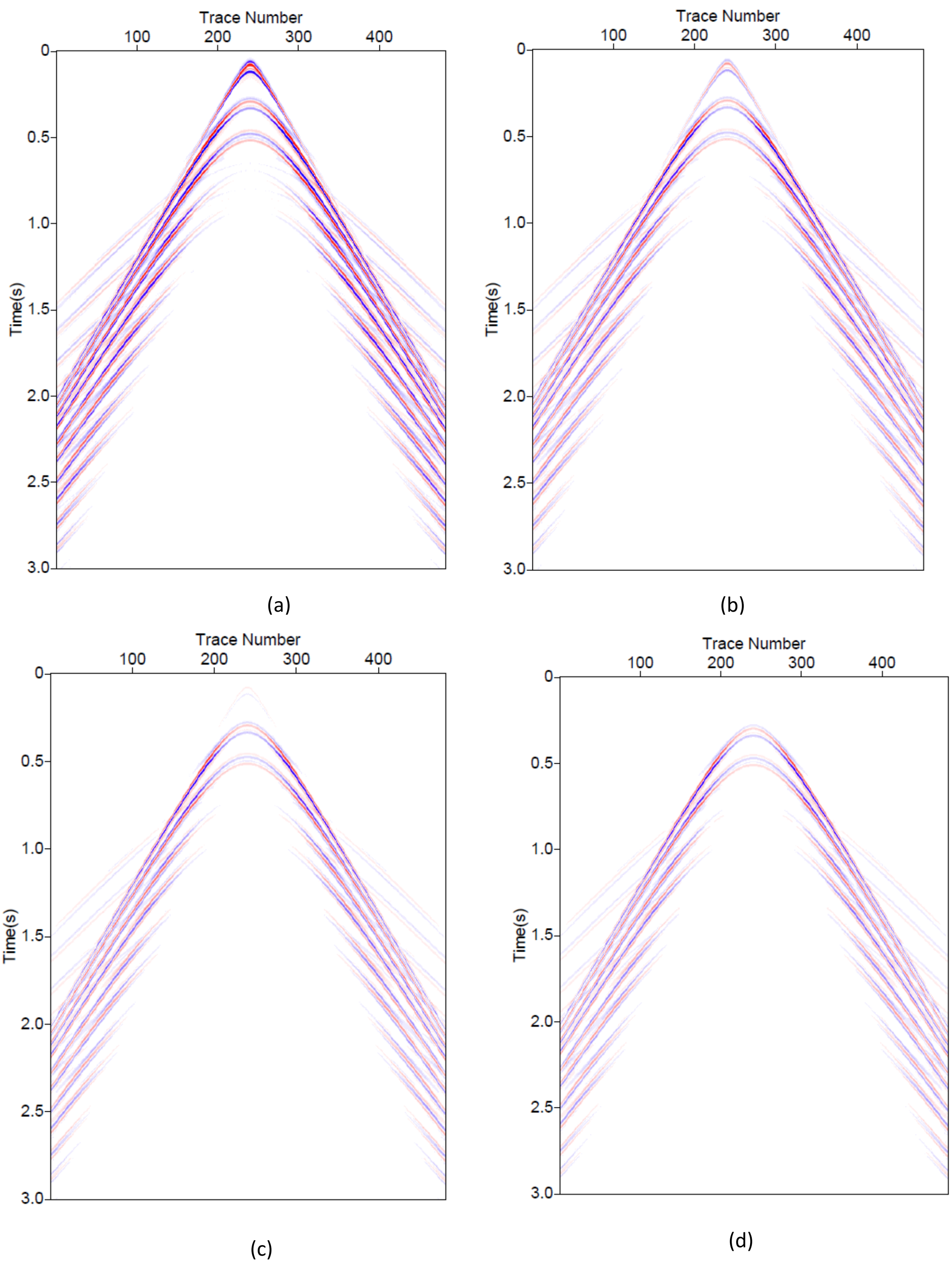

Fig. 2.11: *Predicted P_s when: (a) $\triangle z$ =1/8 $\triangle x$, (b) $\triangle z$ =1/4 $\triangle x$, (c) $\triangle z$ =1/2 $\triangle x$, and (d)$\triangle z = \triangle x$.*

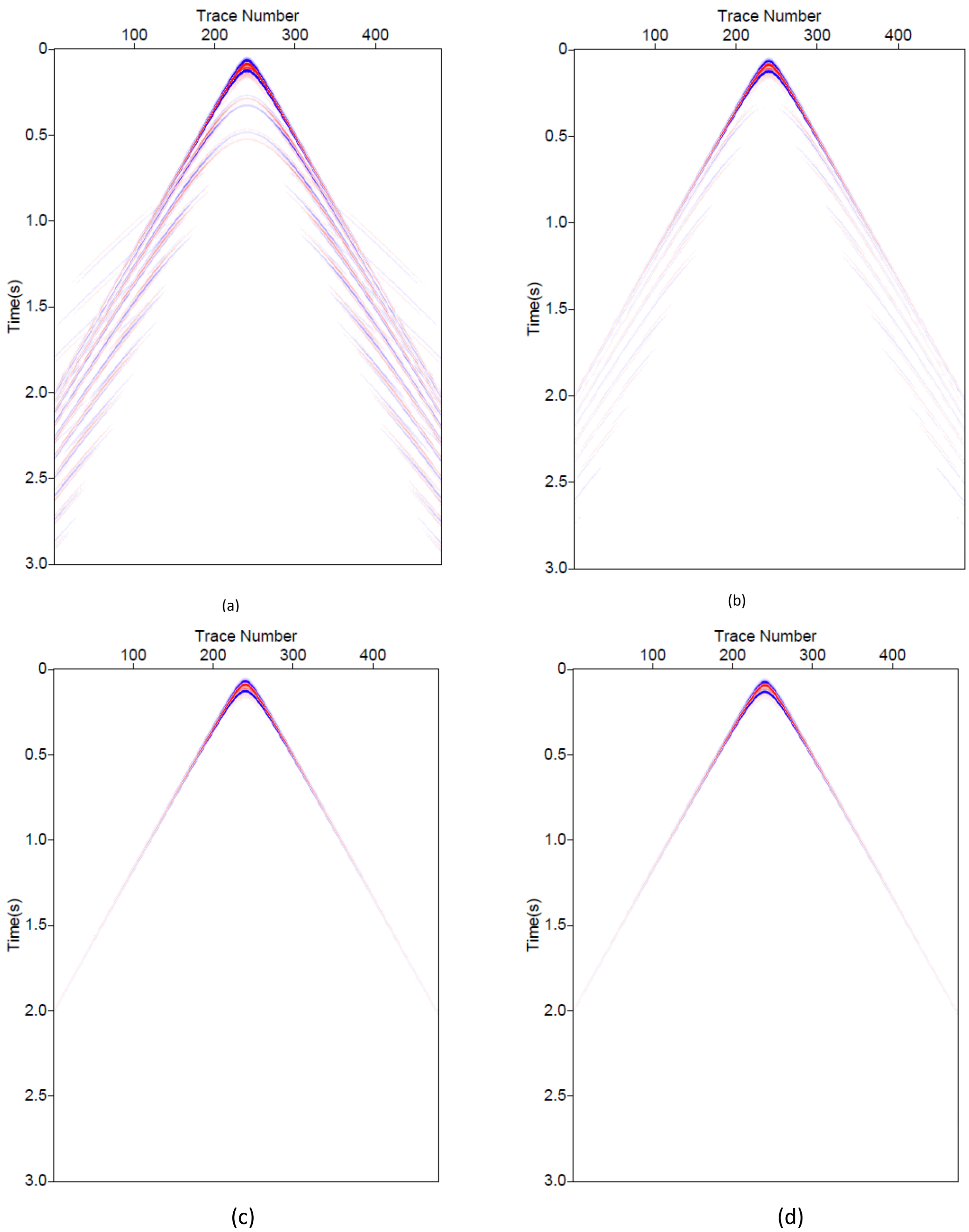

Fig. 2.12: *Predicted P_0 when: (a) $\triangle z$ =1/8 $\triangle x$, (b) $\triangle z$ =1/4 $\triangle x$, (c) $\triangle z$ =1/2 $\triangle x$, and (d)$\triangle z$ = $\triangle x$.*

From (a) to (d), the distance between the prediction point and the cable becomes larger. The results show that, when $\triangle z$ is very small compared with $\triangle x$, the predicted

P_s has many errors (Figure 2.11 (a) and (b)). When $\triangle z$ becomes larger, P_s has fewer errors (Figure 2.11 (c) and (d)). The conclusion is, in order to get a satisfying prediction P_s result, $\triangle z$ is required to be at least half of $\triangle x$. Likewise, Figure 2.12 shows the predicted results of P_0 at different $\triangle z$. Similarly, only when the depth difference between the predicted point and the actual cable $\triangle z$ is larger than 1/2 of the interval between traces, does the predicted direct wave have few residuals.

The reason behind this restriction lies in the form of the Green's function. In 2D marine environments, Green's function and its normal derivative have the forms,

$$G_0(\vec{r},\vec{r'},\omega) = -\frac{i}{4}\left(H_0^{(1)}(kR_+) - H_0^{(1)}(kR_-)\right), \tag{2.8}$$

$$\frac{\partial G_0}{\partial z'}(\vec{r},\vec{r'},\omega) = -\frac{ik}{4}\left(H_1^{(1)}(kR_+)\frac{z-z'}{R_+} + H_1^{(1)}(kR_-)\frac{z+z'}{R_-}\right), \tag{2.9}$$

where $R_\pm = \sqrt{(x-x')^2 + (z \mp z')^2}$. They are plotted in Figure 2.13 as a function of the inline coordinate, x'. The measurement surface is located at depth $z' = 30m$. Different color lines indicate different prediction depths, z. The black line means the prediction point is closest to the cable, and cyan line means the prediction point is far away from the cable. As the prediction point moving away from the cable ($\triangle z$ gets larger), both G_0 and dG_0/dz become more spreading. If we choose the prediction point very close to the cable (*i.e.*, very small $\triangle z$), the Green's function and its normal derivative become very local at one point. In this situation, it becomes impossible to pick up their values in the calculation of the integral in Green's theorem, which will lead to the errors in the prediction of reference wave or scattered wave. Unless having a large $\triangle z$, the calculation of Green's theorem will suffer from this implementation issue. This issue is also observed in deghosting method as mentioned in Weglein *et al.* (2013), in which it purposes the deghosting method in the (k, ω) domain and

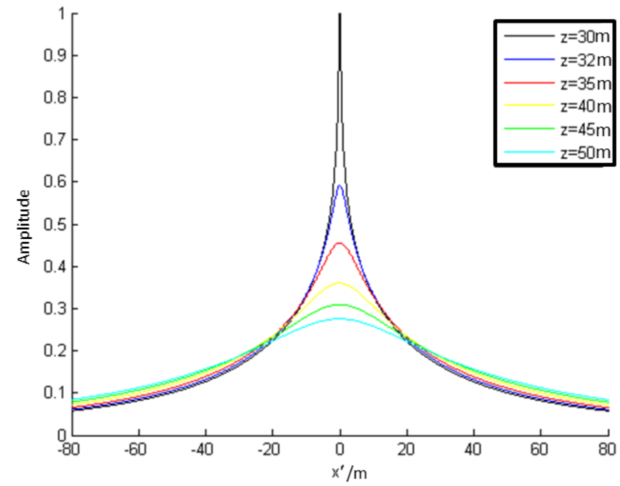

$$G_0(x',z'=30,x=0,z,\omega=25)$$

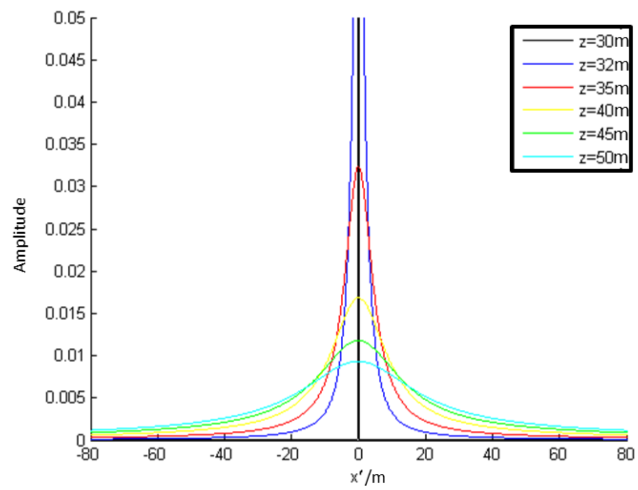

$$\frac{dG_0}{dz}(x',z'=30,x=0,z,\omega=25)$$

Fig. 2.13: *The Green's function (top) and its normal derivative (bottom) as a function of the inline coordinate, x'. The measurement surface is located at depth $z' = 30$ m. Different color lines indicate different prediction depths, z. From the black line to the cyan line, the prediction point is moving far away from the cable.*

compares it with the method in the (x, ω) domain. Likewise, next I will discuss the P_0 P_s wave separation in the (k, ω) domain, which can avoid this implementation issue.

2.4 Wave separation in (k, ω) domain

As mentioned above, the form of Green's function requires us to predict the wavefield P_0 or P_s below or above the measurement surface. In practice, it is often desired to remove the reference wave from the measured data. This issue is especially important for on-shore exploration, where strong ground rolls will be generated at near surface. When the measurement surface is flat, it is possible to simplify the form of Green's theorem into the (k, ω) domain. In this case, we can avoid the implementation issue of Green's function. In this section, the derivation of Green's theorem for wave separation in the (k, ω) domain will be shown using a 2D marine example.

2.4.1 Theory

Assume in a 2D acoustic medium, the cable is placed at depth z', and the prediction point is at depth z. I start the derivation from the P_0 P_s wave separation formula in the (x, ω) domain, which is,

$$\left.\begin{array}{cc} -P_0(x,z,\omega) & when \;\; z > z' \\ P_s(x,z,\omega) & when \;\; z_s < z < z' \end{array}\right\} =$$
$$\int_{m.s.} \left[P(x',z',x_s,z_s,\omega)\frac{\partial}{\partial z'}G_0(x',z',x,z,\omega) - G_0(x',z',x,z,\omega)\frac{\partial}{\partial z'}P(x',z',x_s,z_s,\omega)\right] dx'. \tag{2.10}$$

The negative sign is due to the definition of the positive direction of $\hat{n}$. In order to derive the form in the (k_x, ω) domain, we need to perform Fourier transform on both sides of Equation 2.10 over x. Then the right hand side becomes,

$$\mathrm{RHS} = \iint \{P\frac{\partial}{\partial z'}G_0 - G_0\frac{\partial}{\partial z'}P\}dx' \cdot \exp(-ik_x x)dx. \tag{2.11}$$

Notice that only G_0 and dG_0/dz depend on x. First, let's focus on Fourier transforming $G_0(x', z', x, z, \omega)$ over x.

In the reference medium of half-space air and half-space water separated by a free surface, Green's function $G_0(\vec{r'}, \vec{r}, \omega)$ satisfies,

$$(\nabla'^2 + k^2)G_0(\vec{r'}, \vec{r}, \omega) = \delta(\vec{r'} - \vec{r}) - \delta(\vec{r'} - \vec{r_I}), \tag{2.12}$$

where $\vec{r'} = (x', z')$, $\vec{r} = (x, z)$ and $\vec{r_I} = (x, -z)$. In order to simplify the calculation, I use the plane wave decomposition of G_0, which is the bilinear form,

$$G_0(\vec{r'}, \vec{r}, \omega) = \int \frac{1}{(2\pi)^3}\frac{\exp[i\vec{k'}\cdot(\vec{r'} - \vec{r})] - \exp[i\vec{k'}\cdot(\vec{r'} - \vec{r_I})]}{-\left|\vec{k'}\right|^2 + k^2 + i\varepsilon} \cdot d\vec{k'}. \tag{2.13}$$

The 2D form of Equation 2.13 becomes,

$$\begin{aligned} G_0(x', z', x, z, \omega) &= \frac{1}{(2\pi)^2} \\ &\int \frac{\exp[ik_x{}'(x' - x)][\exp(ik_z{}'(z' - z)) - \exp(ik_z{}'(z' + z))]}{-k_{\mathrm{x}}{}'^2 - k_{\mathrm{z}}{}'^2 + k^2 + i\varepsilon} \cdot dk_x{}'dk_z{}'. \end{aligned} \tag{2.14}$$

Utilizing reciprocity, we have,

$$\begin{aligned} &G_0(x', z', x, z, \omega) = G_0(x, z, x', z', \omega) \\ = &\int \frac{\exp[ik_x{}'(x - x')][\exp(ik_z{}'(z - z')) - \exp(ik_z{}'(z + z'))]}{(2\pi)^2[-k_{\mathrm{x}}{}'^2 - k_{\mathrm{z}}{}'^2 + k^2 + i\varepsilon]} \cdot dk_x{}'dk_z{}'. \end{aligned} \tag{2.15}$$

Now Fourier transform over x with $\int \exp(-ik_x x)dx$,

$$
\begin{aligned}
& \int \exp(-ik_x x) G_0(x', z', x, z, \omega) dx \\
= & \int \underbrace{\int dx \exp(-ik_x x)\exp(ik_x{}' x)}_{2\pi\delta(k_x - k_x{}')} \exp(-ik_x{}' x') \cdot \\
& \frac{\exp(ik_z{}'(z-z')) - \exp(ik_z{}'(z+z'))}{-k_x'^2 - k_z'^2 + k^2 + i\varepsilon} dk_x{}' dk_z{}' \\
= & \exp(-ik_x x') \int \frac{\exp(ik_z{}'(z-z')) - \exp(ik_z{}'(z+z'))}{-k_x{}^2 - k_z'^2 + k^2 + i\varepsilon} dk_z{}' \\
= & \exp(-ik_x x') \frac{\exp(iq|z-z'|) - \exp(iq(z+z'))}{2iq},
\end{aligned} \tag{2.16}
$$

where q satisfies the condition $q^2 = k^2 - k_x^2$. And notice that the absolute value of $z + z'$ is taken off since it's always positive.

So far, we have the form of $G_0(k_x, z, x', z', \omega)$. Next, let's calculate the normal derivative of G_0 by simply differentiating the result of Equation 2.16 with respect of z'.

$$
\begin{aligned}
& \int \exp(-ik_x x) \frac{\partial}{\partial z'} G_0(x', z', x, z, \omega) dx \\
= & \frac{\partial}{\partial z'} \left\{ \exp(-ik_x x') \frac{\exp(iq|z-z'|) - \exp(iq(z+z'))}{2iq} \right\} \\
= & \exp(-ik_x x') [\frac{iq \,\mathrm{sgn}(z'-z) \exp(iq|z-z'|)}{2iq} - \frac{iq \exp(iq(z+z'))}{2iq}] \\
= & \exp(-ik_x x') \frac{\mathrm{sgn}(z'-z) \exp(iq|z-z'|) - \exp(iq(z+z'))}{2}.
\end{aligned} \tag{2.17}
$$

Now plug Equation 2.16 and Equation 2.17 into Equation 2.11, we have

$$
\begin{aligned}
&\text{RHS} = \\
&\int \{P(x',z',x_s,z_s,\omega)\frac{\partial G_0(x',z',k_x,z,\omega)}{\partial z'} - G_0(x',z',k_x,z,\omega)\frac{\partial P(x',z',x_s,z_s,\omega)}{\partial z'}\}dx' \\
&= \int \{\ P(x',z',x_s,z_s,\omega)\left[\exp(-ik_x x')\frac{\text{sgn}(z'-z)\exp(iq|z-z'|) - \exp(iq(z+z'))}{2}\right] \\
&\quad - \left[\exp(-ik_x x')\frac{\exp(iq|z-z'|) - \exp(iq(z+z'))}{2iq}\right] P'(x',z',x_s,z_s,\omega)\ \}\,dx' \\
&= P(k_x,z',x_s,z_s,\omega)\frac{\text{sgn}(z'-z)\exp(iq|z-z'|) - \exp(iq(z+z'))}{2} \\
&\quad -P'(k_x,z',x_s,z_s,\omega)\frac{\exp(iq|z-z'|) - \exp(iq(z+z'))}{2iq}
\end{aligned}
\tag{2.18}
$$

The result of Equation 2.18 depends on the value of $|z-z'|$. When $z > z'$, which means we choose the prediction point below the measurement surface, we have $sgn(z'-z) = -1$. Considering the normal direction of the surface, we have the left hand side,

$$
LHS = -P_0(k_x,z,x_s,z_s,\omega). \tag{2.19}
$$

So, P_0 becomes,

$$
\begin{aligned}
P_0(k_x,z,x_s,z_s,\omega) &= P(k_x,z',x_s,z_s,\omega)\frac{\exp(iq(z-z')) + \exp(iq(z+z'))}{2} \\
&+ P'(k_x,z',x_s,z_s,\omega)\frac{\exp(iq(z-z')) - \exp(iq(z+z'))}{2} \\
&= \frac{(iqP+P')\exp(iq(z-z'))}{2iq} + \frac{(iqP-P')\exp(iq(z+z'))}{2iq}.
\end{aligned}
\tag{2.20}
$$

Similarly, when choosing prediction point above the measurement surface, we have

$z < z'$. So $sgn(z' - z) = 1$. Then,

$$\begin{aligned} P_s(k_x, z, x_s, z_s, \omega) &= P(k_x, z', x_s, z_s, \omega)\frac{\exp\left(iq(z'-z)\right) - \exp\left(iq(z+z')\right)}{2} \\ &- P'(k_x, z', x_s, z_s, \omega)\frac{\exp\left(iq(z'-z)\right) - \exp\left(iq(z+z')\right)}{2} \\ &= \frac{(iqP - P')\exp\left(iq(z'-z)\right)}{2iq} - \frac{(iqP - P')\exp\left(iq(z+z')\right)}{2iq}. \end{aligned} \tag{2.21}$$

Equation 2.20 and Equation 2.21 give the expression of separating the reference wave P_0 and the scattered wave P_s in the (k_x, ω) domain. Notice that in these results $q^2 = \omega^2/c^2 - k_x^2$.

2.4.2 Discussion

Prediction on the cable The calculation in the (k_x, ω) domain enables us to predict P_0 or P_s on the cable, which means isolating the wavefields from the data, rather than predicting them at a different depth. When $z = z' = a$, we can still set the sign of $(z - z')$ as we want, and now we have,

$$P_0(k_x, a, \omega) = \frac{iqP + P'}{2iq} + \frac{(iqP - P')\exp\left(iq2a\right)}{2iq}, \tag{2.22}$$

$$P_s(k_x, a, \omega) = \frac{iqP - P'}{2iq} - \frac{(iqP - P')\exp\left(iq2a\right)}{2iq}. \tag{2.23}$$

As we can see, here

$$P_0 + P_s = P.$$

Wavelet estimation Having P_0, it is also easy to estimate the source signature or radiation pattern. Since

$$P_0(k_x, z, x_s, z_s, \omega) = A(\omega) G_0(k_x, z, x_s, z_s, \omega),$$

and

$$G_0(k_x, z, x_s, z_s, \omega) = \exp(-ik_x x_s) \frac{\exp(iq(z - z_s)) - \exp(iq(z + z_s))}{2iq}. \tag{2.24}$$

The wavelet is,

$$\begin{aligned} A(\omega) &= \frac{P_0(k_x, z, x_s, z_s, \omega)}{G_0(k_x, z, x_s, z_s, \omega)} \\ &= \frac{(iqP + P') \exp(iq(z - z')) + (iqP - P') \exp(iq(z + z'))}{\exp(-ik_x x_s) \left[\exp(iq(z - z_s)) - \exp(iq(z + z_s))\right]}. \end{aligned} \tag{2.25}$$

2.5 Conclusions

In this chapter, the Green's-theorem-based method for separating the reference wave P_0 and the scattered wave P_s is shown in a marine set. The impact of acquisition design (over/under cable) on the wave separation results is also presented. Two factors of the acquisition design that may affect the prediction results are studied: (1) the depth difference between the over/under cable, and (2) the depth difference between the prediction point and the cable.

For the first issue, the closer the two cables are, the more accurate normal derivative of wavefield $\partial P/\partial n$ it will produce from a finite difference approximation. Having the measured wavefields at three cables will help to get more accurate prediction results. Another way to avoid this issue is to construct P and $\partial P/\partial n$ at a depth between the over/under cable using a new Green's function G_0^{DD}, whose value vanishes on both cables.

For the second issue, results show that only when choosing the prediction point away enough from the measurement surface, the wave separation has less errors and satisfying. The reason lies in the form of the Green's function and its normal derivative, which have a very local shape when the prediction point z is chosen to be very close to the cable. In order to predict the wavefield on the cable, or isolate the wavefields of P_0 or P_s from the data, Green's theorem in the (k, ω) domain is introduced. However, it requires a flat measurement surface to perform Fourier transform over the inline coordinate. On the other hand, in the (x, ω) domain, Green's theorem can accommodate non-flat measurement surface, such as in the case of ocean bottom.

3. DETERMINING REFERENCE-MEDIUM PROPERTIES

3.1 Chapter overview

In this chapter, I will show a first step towards extending the prerequisite satisfaction from offshore to land. For seismic exploration on land, one big challenge is to remove the surface wave/reference wave from the reflected data. Because of the complex feature of on-shore near surface medium, understanding of the near surface property becomes a critical issue. This chapter will use marine seismic exploration as a starting point, to illustrate how the invariances in the wavelet estimation can be used as the criteria for predicting the reference medium properties. An analytic example will be shown first to explain the idea of invariances in the wavelet estimation. For a point source, the source wavelet estimated at any point beneath the measurement surface should stay the same, while for a source array, the estimated source wavelet in one radiation angle should be invariant. These invariances could be criteria for verifying that we have the correct reference velocity.

3.2 Introduction

The current trend in the petroleum industry is to explore in deep water and in areas that have complex geology, where primary and multiple events often may be interfering with or proximal to each other. In such cases, removal of the multiple events becomes a big challenge. Inverse Scattering Series (ISS) methods offer a direct way of removing free-surface multiples and attenuating internal multiples without requiring any subsurface information. These methods have prerequisites that need to be satisfied. The prerequisites include identifying and removing the reference wave, estimating the source wavelet and radiation pattern, and deghosting source and receiver. In order to deliver the high fidelity expected of ISS multiple predictions, effective preprocessing methods need to be developed and improved Zhang (2007); Mayhan *et al.* (2011); Mayhan and Weglein (2013); Tang *et al.* (2013); Yang *et al.* (2013).

As seismic exploration moves to increasingly complex and difficult on-shore and off-shore plays, there are additional fundamental issues and challenges that need to be resolved. Among these issues and challenges, removal of the reference wave on land is a pressing and interesting topic. Scattering theory separates the real world into two parts: the reference medium, whose property is known, plus a perturbation. ISS methods require that the reference medium agree with the actual medium on and above the measurement surface. The wave that travels in the reference medium is the reference wave, and it does not experience the earth in its history, so it contains no subsurface information. It is important to identify and remove reference waves before the following data-processing steps.

As mentioned in Section 1.2, in inverse scattering series, the data D on the measurement surface is,

$$\begin{aligned} D &= (G - G_0)_{m.s.} \\ &= G_0 V G \\ &= G_0 V G_0 + G_0 V G_0 V G_0 + ... \end{aligned}$$

As the above equation shows, the very first step of any ISS methods (free surface multiple removal, internal multiple removal and depth imaging) is removing G_0. From the wave equation,

$$L_0 G_0 = \delta,$$

in order to predict and remove G_0, we need to know L_0, which is the reference medium. ISS methods only require the reference medium information to agree with the actual medium at and above the measurement surface. For marine environment, the property of water at the near surface area, where receivers are placed, is relatively easy to define. However, for on-shore seismic applications, the near surface properties are often complicated and difficult to determine. For example, the conditions of rocks, soil or minerals in the near surface are not easy to define due to weathering. Strong ground rolls can be generated, and it can obscure reflected seismic data. To remove the ground roll/reference wave, the physical properties of the near surface is needed.

In order to study the complex on-shore or ocean bottom near surface property, I propose to start from seeking criteria which can determine whether we have the correct reference medium information or not. The criteria could be the presence of some invariance that only the correct reference velocity would satisfy. I use a marine seismic application as a starting point to pursue this idea. First, consider an isotropic point source, which has an isotropic source wavelet in every radiation direction. Green's theorem can estimate the wavelet signature everywhere below the measurement surface. When using the correct reference velocity, the results for the wavelet should be invariant for all output points below the measurement surface. Using this property, the value of reference velocity we use in the wavelet calculation that leads to an invariance of the estimated source wavelet is the correct reference velocity. Furthermore, instead of using a single point source, in practice, source arrays which have angle radiation pattern are widely used in industry (Loveridge *et al.*, 1984). Then the invariance of the estimated wavelet will happen when estimating the wavelet at different points along one radiation angle. Similarly, only the correct reference velocity can lead to the invariance. Thus, the invariances of the source wavelet indicate that we have found the correct reference velocity.

3.3 Theory

3.3.1 Green's theorem for wavelet estimation

Section 1.2 shows the framework of Green's theorem method, and Section 2.2 gives the formula of P_0 P_S wave separation. The source signature information can be extracted once we have the reference wave P_0 predicted from Green's theorem. P_0 can be calculated from Equation 2.1 when choosing prediction point $\vec{r}$ below the measurement surface,

$$P_0(\vec{r}, \vec{r_s}\omega) = \int_{m.s.} \left[P(\vec{r'}, \vec{r_s}, \omega) \frac{dG_0^+(\vec{r}, \vec{r'}, \omega)}{dz} - G_0^+(\vec{r}, \vec{r'}, \omega) \frac{dP(\vec{r'}, \vec{r_s}, \omega)}{dz} \right] \cdot d\vec{r'} \quad (3.1)$$

From the relationship between the reference wave P_0 and source wavelet A given by

Equation 1.18,

$$P_0(\vec{r}, \vec{r_s}, \omega) = A(\omega) G_0^+(\vec{r}, \vec{r_s}, \omega). \tag{3.2}$$

Therefore, source wavelet $A(\omega)$ can be estimated by performing a surface integral and then being divided by the corresponding Green's function.

$$A(\omega) = \frac{1}{G_0^+(\vec{r}, \vec{r_s}, \omega)} \int_{m.s.} \left[P(\vec{r'}, \vec{r_s}, \omega) \frac{dG_0^+(\vec{r}, \vec{r'}, \omega)}{dz} - G_0^+(\vec{r}, \vec{r'}, \omega) \frac{dP(\vec{r'}, \vec{r_s}, \omega)}{dz} \right] \cdot d\vec{r'} \tag{3.3}$$

In marine seismic exploration as shown in Figure 3.1, for the purpose of estimating wavelet, we choose the reference medium as a half-space of air plus a half-space of water. Thus, Green's function consists of two parts,

$$G_0 = G_0^d + G_0^{FS}. \tag{3.4}$$

Equation 3.3 is the equation of the Green's theorem-based wavelet estimation method. $\vec{r'}$ is a point on the measurement surface, and $\vec{r}$ is the prediction point, which needs to be chosen below the measurement surface. This equation is valid for any $\vec{r}$ below the cable. Both the numerator and the denominator of Equation 3.3 are functions of $\vec{r}$, $\vec{r_s}$ and ω. However, their quotient $A(\omega)$ is not a function of the observation point $\vec{r}$. This independence implies that $A(\omega)$ is independent of the prediction point $\vec{r}$. Using this property, we can have the criterion for having the correct reference velocity. A wrong reference velocity in the Green's function will break this property. The quotient will become a function of $\vec{r}$. Next, an analytic example in 1D earth will be shown to illustrate this idea.

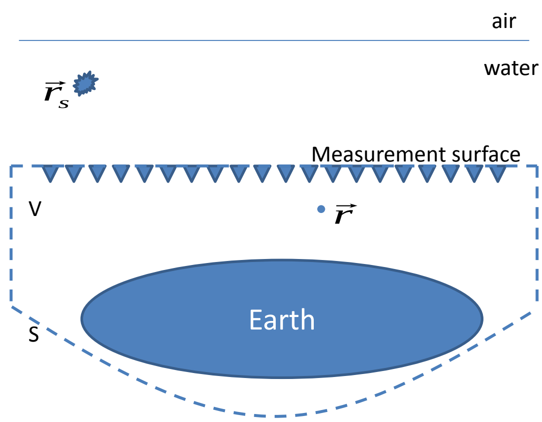

Fig. 3.1: *Marine seismic exploration configuration.*

3.3.2 An analytical example

In this section, an analytical example of wavelet estimation will be given to illustrate the idea of invariance. I start with a 1D example. 1D means the wave propagates only in z direction, and the Earth also only has z direction variance. The configuration is shown in Figure 3.2. Therefore, the "measurement surface" is one point at depth $z' = a$. The surface integral changes to the value of $(P\nabla G_0 - G_0\nabla P)$ at the two ends: infinite $z' = \infty$ and the measurement surface $z' = a$. As discussed above, the prediction point z is chosen as below the measurement surface $z' = a$. Therefore, $z > a > z_s$. The existence of free surface is equal to an image source. Therefore, the Green's function satisfies the wave equation,

$$(\frac{d^2}{dz^2} + k^2)G_0(z, z', \omega) = \delta(z - z') - \delta(z + z'). \tag{3.5}$$

So Green's function G_0 and its normal derivative dG_0/dz' in 1D are,

$$\begin{aligned} G_0(z,z',\omega) &= \frac{\exp(ik|z-z'|)}{2ik} \\ &= \frac{\exp(ik(z-z')) - \exp(ik(z+z'))}{2ik}, \qquad (3.6) \\ \frac{d}{dz'}G_0(z,z',\omega) &= \frac{-\exp(ik(z-z')) - \exp(ik(z+z'))}{2}. \qquad (3.7) \end{aligned}$$

In this example, there is no perturbation below the measurement surface. Therefore, the measured wavefield P equals the reference wave P_0. On the measurement surface $z' = a$, the wavefield P and its normal derivative dP/dz' are,

$$\begin{aligned} P(z',z_s,\omega) &= A(\omega)G_0(z',z_s,\omega) \\ &= A(\omega)\frac{\exp(ik(z'-z_s)) - \exp(ik(z'+z_s))}{2ik}, \qquad (3.8) \\ \frac{d}{dz'}P(z',z_s,\omega) &= A(\omega)\frac{d}{dz'}G_0(z',z_s,\omega) \\ &= A(\omega)\frac{\exp(ik(z'-z_s)) - \exp(ik(z'+z_s))}{2}. \qquad (3.9) \end{aligned}$$

So the predicted reference wave $P_0(z,z_s,\omega)$ is,

$$\begin{aligned} P_0(z,z_s,\omega) &= |_{z'=a}^{\infty}\left[(z',z_s,\omega)\frac{d}{dz'}G_0(z,z',\omega) - G_0(z,z',\omega)\frac{d}{dz'}P(z',z_s,\omega)\right] \\ &= 0 - \left[A(\omega)\frac{[\exp(ik(a-z_s)) - \exp(ik(a+z_s))]}{2ik}\frac{[-\exp(ik(z-a)) - \exp(ik(z+a))]}{2}\right. \\ &\quad \left. - \frac{[\exp(ik(z-a)) - \exp(ik(z+a))]}{2ik}A(\omega)\frac{[\exp(ik(a-z_s)) - \exp(ik(a+z_s))]}{2}\right] \\ &= A(\omega)\frac{1}{2ik}[\exp(ik(z-z_s)) - \exp(ik(z+z_s))]. \qquad (3.10) \end{aligned}$$

Therefore,

$$\frac{P_0(z,z_s,\omega)}{G_0(z,z_s,\omega)} = \frac{A(\omega)\frac{1}{2ik}[\exp(ik(z-z_s)) - \exp(ik(z+z_s))]}{\frac{1}{2ik}[\exp(ik(z-z_s)) - \exp(ik(z+z_s))]} = A(\omega) \tag{3.11}$$

The above equation shows that even though both P_0 and G_0 depend on the prediction point z, their quotient $A(\omega)$ is independent of z. When a wrong reference velocity c_0' is used to predict the wavelet, Green's functions in the above equation contains a wrong wavenumber $k' = \omega/c_0'$. We now have,

$$\begin{aligned} P_0(z,z_s,\omega) = \ & |_{z'=a}^{\infty} P(z',z_s,\omega)\tfrac{d}{dz'}G_0(z,z',\omega) - G_0(z,z',\omega)\tfrac{d}{dz'}P(z',z_s,\omega) \\ = 0 - \Bigg[& A(\omega)\frac{[\exp(ik(a-z_s)) - \exp(ik(a+z_s))]}{2ik}\frac{[-\exp(ik'(z-a)) - \exp(ik'(z+a))]}{2} \\ - & \frac{[\exp(ik'(z-a)) - \exp(ik'(z+a))]}{2ik'}A(\omega)\frac{[\exp(ik(a-z_s)) - \exp(ik(a+z_s))]}{2}\Bigg] \\ = A(\omega)(&\frac{1}{4ik} + \frac{1}{4ik'})[\exp(i(k'z - kz_s + (k-k')a)) - \exp(i(k'z + kz_s) + (k-k')a))]. \end{aligned} \tag{3.12}$$

So the wavelet becomes,

$$\begin{aligned} & \frac{P_0(z,z_s,\omega)}{G_0(z,z_s,\omega)} \\ = & \frac{A(\omega)(\frac{1}{4ik} + \frac{1}{4ik'})[\exp(i(k'z - kz_s + (k-k')a)) - \exp(i(k'z + kz_s) + (k-k')a))]}{\frac{1}{2ik'}[\exp(ik'(z-z_s)) - \exp(ik'(z+z_s))]} \end{aligned} \tag{3.13}$$

Now using the wrong reference velocity to calculate the wavelet, the result of $A(\omega)$ depends on the observation point z. So the property of invariance no longer exists. By observing the invariance of predicted wavelet at different output points under the cable, we can determine if we have the correct reference velocity or not. We use an marine environment as an example to test this idea.

Discussion In order to better illustrate the idea and keep it simple, the above 1D example has included a free surface. If we remove the free surface, then both wavefield P and the Green's function G_0 have only the first term. Now in the result of using a wrong reference velocity, the prediction point, which only depends on z, will be canceled in the above equation. Equation 3.12 now becomes,

$$\begin{aligned}
& P_0(z, z_s, \omega) \\
= \; & |_{z'=a}^{\infty} P(z', z_s, \omega) \frac{d}{dz'} G_0(z, z', \omega) - G_0(z, z', \omega) \frac{d}{dz'} P(z', z_s, \omega) \\
= \; & 0 - \left[A(\omega) \frac{\exp(ik(a - z_s))}{2ik} \frac{-\exp(ik'(z-a))}{2} \right. \\
& \left. - \frac{\exp(ik'(z-a))}{2ik'} A(\omega) \frac{\exp(ik(a-z_s))}{2} \right] \\
= \; & A(\omega)(\frac{1}{4ik} + \frac{1}{4ik'})[\exp(i(k'z - kz_s + (k-k')a))]. \qquad (3.14)
\end{aligned}$$

Dividing a Green's function with the wrong wavenumber k', the wavelet becomes,

$$\begin{aligned}
\frac{P_0(z, z_s, \omega)}{G_0(z, z_s, \omega)} &= \frac{A(\omega)(\frac{1}{4ik} + \frac{1}{4ik'})[\exp(i(k'z - kz_s + (k-k')a))]}{\frac{1}{2ik'}[\exp(ik'(z - z_s))]} \\
&= A(\omega) \frac{k' + k}{2k} \exp[i(k - k')(a - z_s)]. \qquad (3.15)
\end{aligned}$$

Even though the above wavelet result is not correct, it is no longer dependent with the prediction point z. Does it mean that the invariance no longer holds? No. The reason is that our assumption has assumed a 1D world. If we analyze the problem in 2D or 3D without free surface, we can do it in the (k, ω) domain as in Section 2.4, using a bilinear form of Green's function. Equation 2.16 gives the 2D Green's function in (k_x, ω) domain. When there is no free surface, it is,

$$G_0(k_x, z, x', z', \omega) = \exp(-ik_x x') \frac{\exp(iq|z - z'|)}{2iq}, \tag{3.16}$$

where q satisfies the condition $q^2 = k^2 - k_x^2$. This form is exactly the same form with the 1D Green's function, except that k becomes q. Now, it is clear that the estimated wavelet, if using a wrong reference velocity, will have the same form of Equation 3.15, with the replacement of k to be q. The result is still independent of z, but it is actually dependent of the coordinate x. How do we know it? If it is independent of x, then the form in (k_x, ω) domain should be in the form of $\delta(k_x)$. But it is not. So it is actually dependent of the prediction point (x, z). To avoid this complicated analysis, in the beginning of this section I used the simple example of 1D with free surface to illustrate the idea.

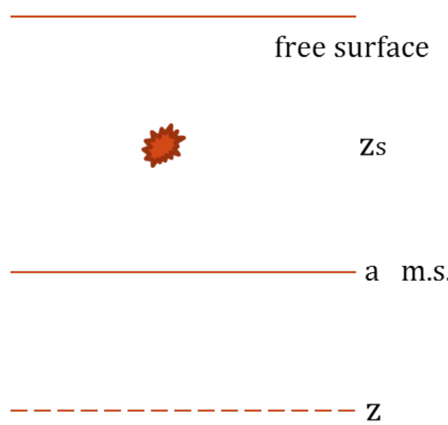

Fig. 3.2: *A 1D example*

3.3.3 Radiation pattern

In the previous section, we focused on solving the wavelet from a point source at $\delta(\vec{r}-\vec{r_s})$. In a more general case, an extended source array that consists of several point source could be used in seismic exploration. In this case, the source displays a radiation pattern in different radiation angles. The radiation pattern from a single effective point source could be estimated by assuming that $A(\omega)$ is a function of the radiation angle θ (using far field approximation).

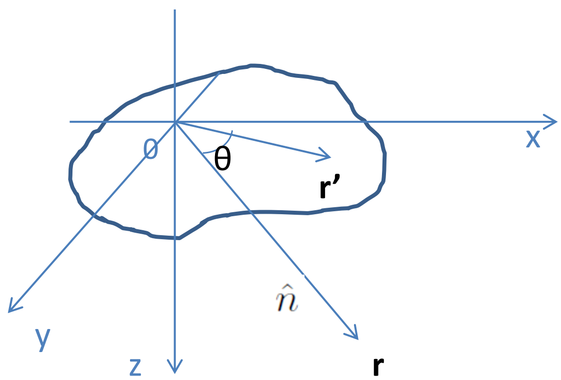

Fig. 3.3: *A general extended source.*

Figure 3.3 shows an example of a general extended source $\rho(\vec{r})$. Wavefield at $\vec{r}$ generated from this source array can be calculated from the integral,

$$P_0(\vec{r},\omega) = \int G_0(\vec{r},\vec{r'},\omega)\rho(\vec{r'})d\vec{r'}. \tag{3.17}$$

In 3D propagation, Green's function in frequency domain can be written as

$$G_0(\vec{r},\vec{r'},\omega) = \frac{e^{ik|\vec{r}-\vec{r'}|}}{|\vec{r}-\vec{r'}|}. \tag{3.18}$$

In the far field, $|\vec{r}| >> |\vec{r'}|$, we have approximation,

$$
\begin{aligned}
|\vec{r}-\vec{r'}| &= \sqrt{(\vec{r}-\vec{r'})^2} \\
&= \sqrt{r^2 - 2\vec{r}\cdot\vec{r'} + r'^2} \\
&= r[1 - \frac{2\vec{r}\cdot\vec{r'}}{r^2} + \frac{r'^2}{r^2}]^{1/2} \\
&= r(1 - \frac{\vec{r}\cdot\vec{r'}}{r^2} + \frac{r'^2}{2r^2} + ...) \\
&= r - \hat{n}\cdot\vec{r'} + O(\frac{1}{r}).
\end{aligned} \tag{3.19}
$$

The above equation uses Taylor series $(1+x)^{1/2} = 1 + \frac{1}{2}x + O(x^2)$, and $\hat{n}$ is the unit vector in the direction of $\vec{r}$. And similarly,

$$
\frac{1}{|\vec{r}-\vec{r'}|} = \frac{1}{r} + \frac{\hat{n}\cdot\vec{r'}}{r^2} + ... = \frac{1}{r} + O(\frac{1}{r^2}). \tag{3.20}
$$

Then in the far field, Equation 3.17 becomes

$$
\begin{aligned}
P_0(\vec{r},\omega) &= \int \frac{e^{ik(r-\hat{n}\cdot\vec{r'})}}{r}\rho(\vec{r'})d\vec{r'} \\
&= \frac{e^{ikr}}{r}\int e^{-ik\hat{n}\cdot\vec{r'}}\rho(\vec{r'})d\vec{r'} \\
&= \frac{e^{ikr}}{r}\tilde{\rho}(k\hat{n}).
\end{aligned} \tag{3.21}
$$

Therefore, if we treat seismic data generated from an extended source as if from a point source, we can get the source wavelet,

$$
A(\omega,\theta) = \frac{P_0(\vec{r},\omega)}{G_0(\vec{r},\omega)} = \tilde{\rho}(k\hat{n}).
$$

Since $\hat{n}$ is the direction from the source to the observation point, the estimated wavelet result will display variances in different radiation angle. However, in one radiation angle $\hat{n}$, wavelet $A(\omega, \theta)$ will be the same. This could be used as a criterion for determining the correct reference velocity. If using a wrong reference velocity, this invariance at one radiation angle will not be satisfied. The property of invariances at one radiation angle will be broken. I will examine this property in the synthetic test.

3.4 Point source

In this test, we use the Cagnidard-de Hoop method to model over-under cable data. Then using the Green's theorem of Equation 3.3, we estimate wavelet $A(\omega)$, at different points at a fixed depth. We predict the estimated wavelet results by using different reference velocities:

(1) the correct reference velocity $c_0 = 1500$ m/s;

(2) a wrong reference velocity $c_0 = 1490$ m/s;

(3) an additional wrong reference velocity $c_0 = 1450$ m/s.

The estimated reference wavefields P_0 are shown in Figure 3.4, and the corresponding wavelet are presented in Figure 3.5. Figure 3.4 indicates that the wrong reference velocities also lead to errors in the prediction of P_0. The estimated source wavelet results show that when using the correct reference velocity, the wavelet displays invariance at different offset, while wrong velocities give different wavelet prediction at different output points.

Therefore, only the correct reference velocity can result in the invariance of the estimated wavelet. When the reference velocities become progressively more incorrect, the errors of the wavelet invariance also becomes larger. This conclusion will also help us in finding the correct reference velocity.

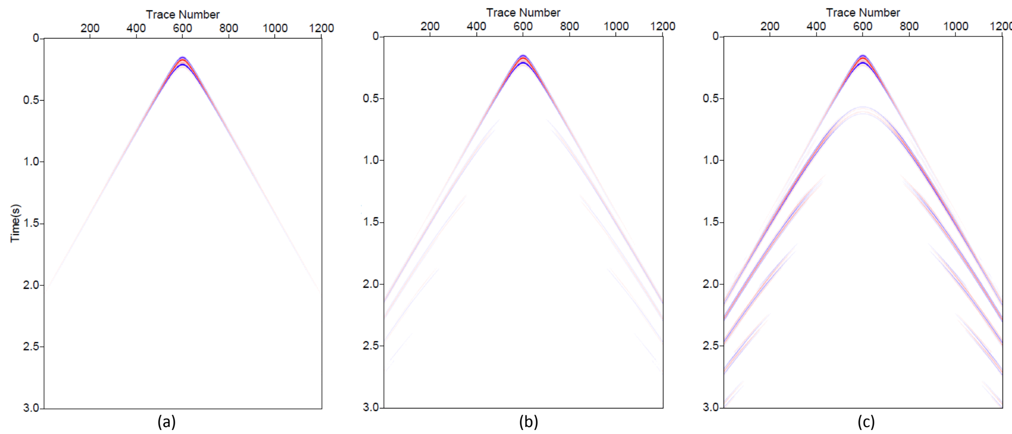

Fig. 3.4: *P_0 estimated using (a) correct $c_0 = 1500$ m/s, (b) wrong $c_0 = 1490$ m/s, (c) wrong $c_0 = 1450$ m/s*

3.5 Source array

In this section, instead of using a point source, I will test data generated by a source array. The source array consists of 7 point sources separated at 3 m, as shown in Figure 3.6. First, we will estimate source wavelet along a horizontal cable, whose radiation angles are different. We predict source wavelet at depth 56m, from offset 0 m to 606 m, whose radiation angles are from 0° to 85°. The results in Figure 3.7 show the radiation pattern in different offset (radiation angle). Next, we estimate the wavelet $A(\omega, \theta)$ in one radiation angle. The estimated wavelet results in angle 5.8°, using both the correct reference velocity (1500 m/s) and the wrong reference velocity (1450 m/s), are shown in Figure 3.8. From these results, we can see that

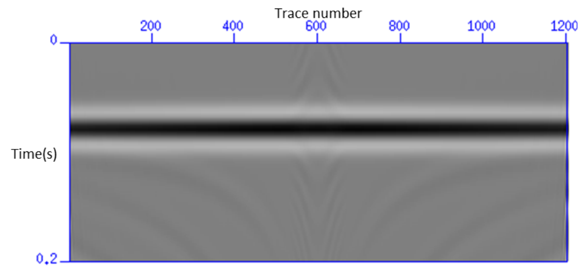

(a)

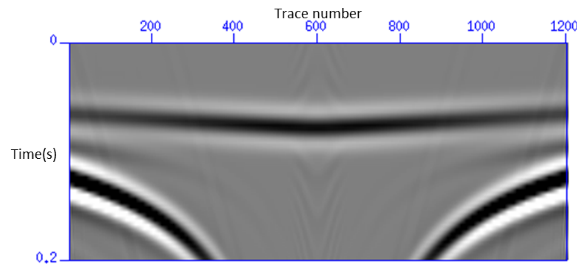

(b)

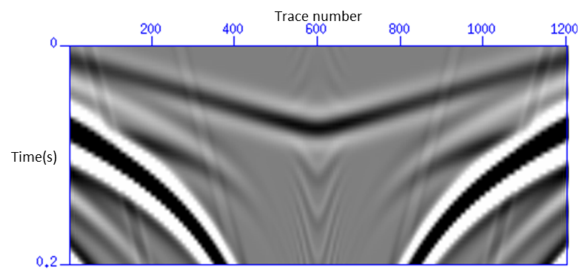

(c)

Fig. 3.5: *$A(t)$ estimated using (a) correct $c_0 = 1500$ m/s, (b) wrong $c_0 = 1490$ m/s, and (c) wrong $c_0 = 1450$ m/s*

only when using the correct reference velocity, we can observe the invariance of the source array wavelet in one radiation angle, whereas the wrong reference velocity will lead to differences in the wavelet estimation along one radiation angle.

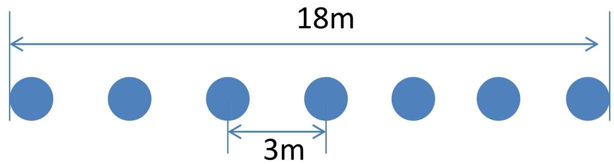

Fig. 3.6: *Source array*

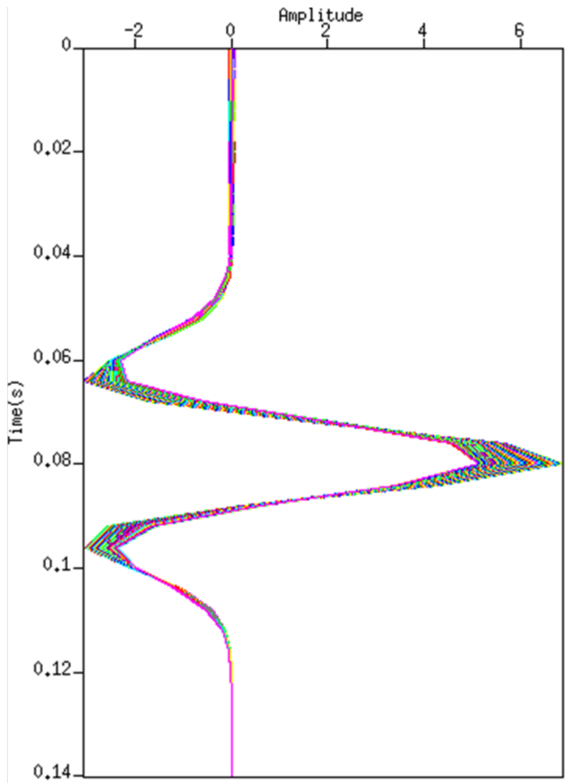

Fig. 3.7: *Radiation pattern of the source array in Figure 3.6, estimated from offset 0 m to 606 m.*

3.6 Conclusions

This chapter has shown that the invariances of a wavelet estimated by using Green's theorem could be a criterion for determining the correct reference velocity. For a point source, the invariance occurs for the output points anywhere below the measurement surface, while for a source array, the invariance is for output points along one radiation

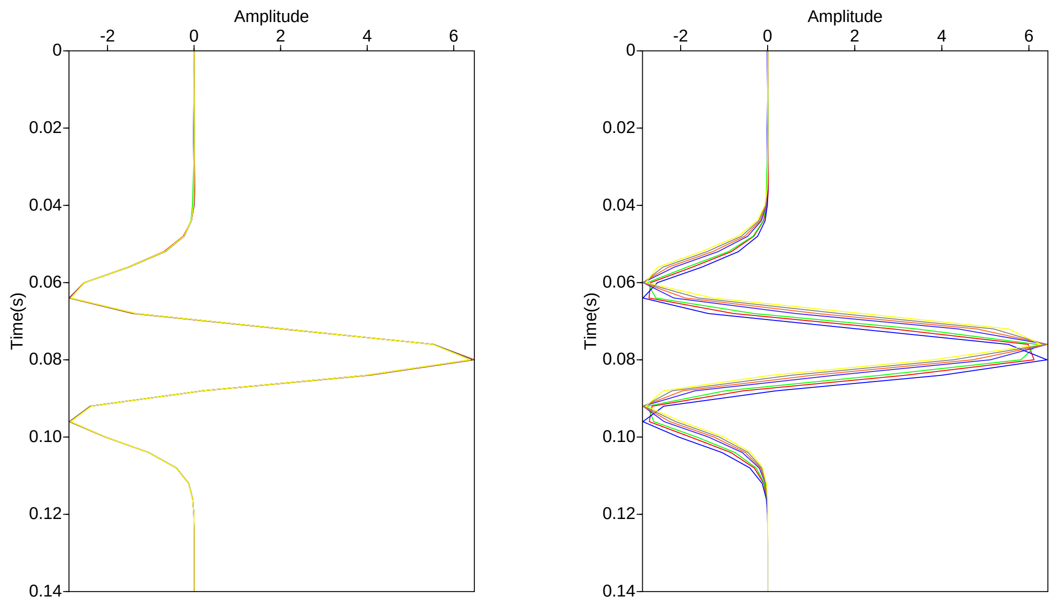

(a) (b)

Fig. 3.8: *Wavelet estimated at depths 36 m, 56 m, 76 m, 96 m, 116 m, 136 m, and 156 m, at the same radiation angle and using (a) the correct reference wave* $c_0 = 1500$ *m/s and (b) a wrong reference velocity* $c_0 = 1450$ *m/s.*

angle. This idea is illustrated using a marine seismic application as a starting point. Using a similar thinking, in the future study we will focus on solving the complex on-shore or ocean-bottom near surface medium problems. For complex on-shore or ocean bottom problems, understanding of the near surface property could enable us to predict and remove the ground roll/reference wave on land, and thereby enhance the capability of subsequent multiple removal processing steps for the challenge of on-shore multiple attenuation.

4. STUDY OF WAVELET ESTIMATION METHODS

4.1 Chapter overview

Source-signature estimation is an important step in seismic exploration. The knowledge of source signature is essential to identify and remove the contribution of the source from the recorded data. It is needed in many steps of seismic data processing, such as multiple removal and ISS depth imaging. In this chapter, I focus the discussion on comparing different methods for wavelet estimation. Three methods will be introduced step by step: (1) the Wiener-filter method, (2) the spectral-division method and (3) the Green's-theorem method. The relationship of these methods will be discussed. Synthetic data, both with and without noise, will be tested using the three methods. Results show that all three methods can predict the source wavelet very well when the data set contains no noise. When the data contains noise, the Green's-theorem method demonstrates strength, since it utilizes an integral along the measurement surface, which tends to reduce random noise. In addition, a marine field data set, Kristin data, will be tested using the Wiener filter method. The result of the source wavelet is used in the first field data test of ISS depth imaging for the purpose of data regularization.

4.2 Wavelet estimation methods

4.2.1 Wiener filter method

The Wiener filter method, developed by Norbert Wiener (Wiener, 1949), has great practical use for implementation in many fields of signal data processing, such as linear prediction, channel equalization and system identification (Robinson and Treitel, 1980; Vaseghi, 2008). It is typically used when given the inputs and outputs of a system, to estimate the character of the system, or in the estimation of a signal observed in noise. The objective criterion of Wiener filter is the least-mean-square error between the filter output and the desired signal. The coefficients of the filter are obtained by minimizing the average squared-error function with respect of the filter coefficients. The solution of the coefficients uses the information of the autocorrelation of the input and the cross-correlation of the input and the desired signal. This powerful method provides us an approach of doing deconvolution robustly in the time domain, which avoids the instability of a division. Also, with the length of the filter given as a priori information, the predicted result is very stable.

For seismic exploration, the Wiener filter method can extract a wavelet from the reference wave and the reference Green's function. This method has straightforward physical meaning and does not involve complicated numerical calculation.

In the case of surface marine seismic, the separation between the reference and scattered fields depends on the depth of the water bottom. If the water is sufficiently deep, the reference and scattered fields do not interfere, and it is possible to estimate the wavelet by deconvolving the reference wavefield by the Green's function of the reference medium.

In this section I will first introduce the necessary background of convolutional model, and then present the theory of Wiener filter method. These sections are extracted from Sheriff and Geldart (1994) and Robinson and Treitel (1980) with different signal notations for a better understanding of our specific application. Next, the comparison and relationship of Wiener filter method and the spectral division method are discussed.

When the source signature is an impulsive spike $\delta(t)$ at $\vec{r_s}$, what the receiver at $\vec{r}$ record will be the Green's function. Assume the source is a point source, $\rho(\vec{r},t) = A(t)\delta(\vec{r}-\vec{r_s})$. Also assuming the wavelet $A(t)$ has a finite length time, we can break it up into a sum of a set of impulsive functions in time, which means

$$A(t) = \int_{-\infty}^{\infty} A(\tau)\delta(t-\tau)d\tau. \tag{4.1}$$

Assuming the linearity and time-invariance of the earth, the response would become

$$P(\vec{r},\vec{r_s},t) = \int_{-\infty}^{\infty} A(\tau)G(\vec{r},\vec{r_s},t-\tau)d\tau. \tag{4.2}$$

The contribution to the recorded trace at time t from the portion of wavelet at time τ is $A(\tau)G(t-\tau)$. The total of response at t is the sum of all times within the wavelet. The length of the recorded data is the sum of wavelet and the Green's function.

The Equation 4.2 can also be derived in the frequency domain. Assuming source $\rho(\vec{r},\omega)$ and Green's function $G(\vec{r},\vec{r}',\omega)$, the wavefield would be

$$P(\vec{r},\vec{r_s},\omega) = \int_{-\infty}^{\infty} d\vec{r}'\rho(\vec{r}',\omega)G(\vec{r},\vec{r}',\omega) \tag{4.3}$$

Assuming the source is a point source, $\rho(\vec{r},\omega) = A(\omega)\delta(\vec{r}-\vec{r}_s)$, we can obtain,

$$P(\vec{r},\vec{r}_s,\omega) = A(\omega)G(\vec{r},\vec{r}_s,\omega) \tag{4.4}$$

Equation 4.2 and Equation 4.4 are the same relation presented in different domain. A Fourier transform over t of Equation 4.2 will give us Equation 4.4.

$$\begin{aligned}
& \int_{-\infty}^{\infty} e^{i\omega t}dt \int_{-\infty}^{\infty} A(\tau)G(\vec{r},\vec{r}_s,t-\tau)d\tau && (4.5)\\
\xrightarrow{t-\tau=s} & \int_{-\infty}^{\infty} e^{i\omega s}ds \int_{-\infty}^{\infty} A(\tau)G(\vec{r},\vec{r}_s,s)e^{i\omega t}d\tau && (4.6)\\
= & \int_{-\infty}^{\infty} G(\vec{r},\vec{r}_s,s)e^{i\omega s}ds \int_{-\infty}^{\infty} A(\tau)e^{i\omega t}d\tau && (4.7)\\
= & \; G(\vec{r},\vec{r}_s,\omega)A(\omega) && (4.8)
\end{aligned}$$

In scattering theory, we treat the actual medium as a combination of an unperturbed medium, called the reference medium, plus a perturbation. According to the convolutional model, in the reference medium world, the wavefield P_0 is the convolution of the wavelet $A(t)$ with the reference Green's function G_0, so

$$P_0(\vec{r},\vec{r}_s,t) = \int_{-\infty}^{\infty} A(\tau)G_0(\vec{r},\vec{r}_s,t-\tau)d\tau. \tag{4.9}$$

The reference wave P_0 can be extracted directly from raw data where P_0 and the scattered wave P_s do not overlap. The reference Green's function G_0 can be calculated from the wave equation easily once we defined the reference medium as a half space of air plus a half space of water in the marine set.

To solve wavelet $A(t)$ from Equation 4.9, one possible solution is to convert this equation to the frequency domain, which becomes

$$P_0(\vec{r}, \vec{r}_s, \omega) = A(\omega) G_0(\vec{r}, \vec{r}_s, \omega), \tag{4.10}$$

so that wavelet in frequency domain can be solved by a division of $P_0(\vec{r}, \vec{r}_s, \omega)$ and $G_0(\vec{r}, \vec{r}_s, \omega)$. However, to avoid the instability issues caused by the division, I use the Wiener filter method to calculate wavelet $A(t)$ in the time domain.

Using the Wiener filter method, we treat the wavelet $A(t)$ as a shaping filter that shapes the input signal (Green's function $G_0(\vec{r}, \vec{r}_s, t)$) to be the desired signal (reference wave $P_0(\vec{r}, \vec{r}_s, t)$), as shown in Figure 4.1.

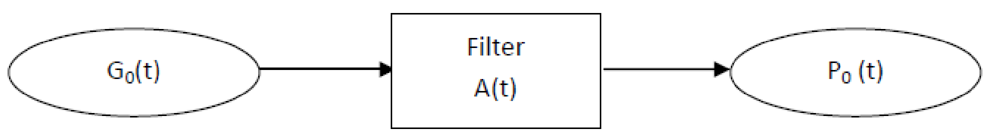

Fig. 4.1: *Wavelet $A(t)$ is treated as a filter that shapes the Green's function to be the reference wave.*

The Wiener filter method uses a least-square criterion to find the "best" filter. Suppose that we have an input signal $G_0(t)$ and a filter $A(t)$, which together give an output signal $X(t)$. While we need output $P_0(t)$, the difference between then are defined as error $E(t)$.

$$X(t) = \int_{-\infty}^{\infty} A(\tau) G_0(t-\tau) d\tau = A(t) * G_0(t) \tag{4.11}$$

$$E(t) = P_0(t) - X(t) \tag{4.12}$$

Here $*$ means convolution. In the actual seismic data processing, functions are discrete number series. So from now on, I use the discrete expression. Assume that the filter

A is a series $(A_0, A_1, A_2, ..., A_m)$, the input Green's function is $(G_0, G_1, G_2, ..., G_n)$, and the desired P wave is $(P_0, P_1, P_2, ..., P_{m+n})$, so that

$$X_t = \sum_{s=0}^{m} A_s G_{t-s} \qquad t = 0, 1, 2, ..., m+n. \tag{4.13}$$

$$E_t = P_t - X_t = P_t - \sum_{s=0}^{m} A_s G_{t-s} \qquad t = 0, 1, 2, ..., m+n. \tag{4.14}$$

In order to have the output signal close to the desired function, we need to minimize the energy of error, which is defined as I,

$$I = \sum_{t=0}^{m+n} E_t^2 \tag{4.15}$$

$$= \sum_{t=0}^{m+n} (P_t - \sum_{s=0}^{m} A_s G_{t-s})^2. \tag{4.16}$$

Here we are looking for a least-square error with the choice of filter coefficients A_n, which corresponds to the Wiener filter. So the partial derivative of error energy with each coefficients of filter should be zero, *i.e.*,

$$\frac{\partial I}{\partial A_i} = 0 \qquad i = 0, 1, 2, ..., m. \tag{4.17}$$

An example of A_0 shows

$$
\begin{aligned}
\frac{\partial I}{\partial A_0} &= \frac{\partial}{\partial A_0}\left[\sum_{t=0}^{m+n}(P_t - \sum_{s=0}^{m} A_s G_{t-s})^2\right] && (4.18)\\
&= \sum_{t=0}^{m+n}\left[\frac{\partial}{\partial A_0}(P_t - \sum_{s=0}^{m} A_s G_{t-s})^2\right] && (4.19)\\
&= \sum_{t=0}^{m+n}\left[2(P_t - \sum_{s=0}^{m} A_s G_{t-s})\right]\left[-\frac{\partial}{\partial A_0}(\sum_{s=0}^{m} A_s G_{t-s})\right] && (4.20)\\
&= 2\sum_{t=0}^{m+n}\left[(P_t - \sum_{s=0}^{m} A_s G_{t-s})(-G_t)\right] && (4.21)\\
&= 2\left[-\sum_{t=0}^{m+n} P_t \cdot G_t + \sum_{s=0}^{m} A_s \cdot (\sum_{t=0}^{m+n} G_{t-s} G_t)\right] && (4.22)\\
&= 0. && (4.23)
\end{aligned}
$$

So we have,

$$\sum_{s=0}^{m} A_s \cdot (\sum_{t=0}^{m+n} G_{t-s} G_t) = \sum_{t=0}^{m+n} P_t \cdot G_t. \tag{4.24}$$

Now we start using the concept of correlation, which measures the similarity of two functions (Sheriff and Geldart, 1994). It also shows how the similarity varies as we shift one trace with respect of the other. The mathematical definition of cross-correlation $\phi_{xy}(\tau)$ of two functions x_t and y_t is

$$\phi_{xy}(\tau) = \sum_{t=0} x_{t+\tau} y_t. \tag{4.25}$$

The definition implies that we shift the function x over the other by τ, then multiply the corresponding part of the two functions and sum up for each value of t. The larger $\phi(\tau)$ is, the more similar the two signals are at lag τ. Likewise, auto-correlation measures how a function correlates with itself shifted in a time, defined as

$$\phi_{xx}(\tau) = \sum_{t=0} x_{t+\tau} x_t. \tag{4.26}$$

Back to Equation 4.24, we use the correlation of input G_t and desired signal P_t and the auto-correlation of G_t as

$$\begin{aligned} \phi_{PG}(0) &= \sum_{t=0}^{m+n} P_t \cdot G_t & (4.27) \\ \phi_{GG}(s) &= \phi_{GG}(-s) = \sum_{t=0}^{m+n} G_{t-s} G_t. & (4.28) \end{aligned}$$

Notice that auto-correlation is an even function. Equation 4.24 becomes,

$$\sum_{s=0}^{m} A_s \cdot \phi_{GG}(s) = \phi_{PG}(0). \tag{4.29}$$

Equation 4.29 comes from the partial derivative of error energy by the first coefficient A_0 of filter. Similar results can be obtained from the remaining differential equations of Equation 4.17, which implies,

$$\sum_{s=0}^{m} A_s \cdot \phi_{GG}(i-s) = \phi_{PG}(i) \qquad i = 0, 1, 2, ..., m. \tag{4.30}$$

The above equations can be written in a matrix form, which is,

$$\begin{bmatrix} \phi_{GG}(0) & \phi_{GG}(1) & ... & \phi_{GG}(m) \\ \phi_{GG}(1) & \phi_{GG}(0) & ... & \phi_{GG}(m-1) \\ \vdots & \vdots & \vdots & \vdots \\ \phi_{GG}(m) & \phi_{GG}(m-1) & ... & \phi_{GG}(0) \end{bmatrix} \begin{bmatrix} A_0 \\ A_1 \\ \vdots \\ A_m \end{bmatrix} = \begin{bmatrix} \phi_{PG}(0) \\ \phi_{PG}(1) \\ \vdots \\ \phi_{PG}(m) \end{bmatrix}. \tag{4.31}$$

The above set of equations are the most important relationship in Wiener filter method. From these equations, the filter A_t can be solved by using Toeplitz recursion (Robinson and Treitel, 1980). The detailed steps of Wiener filter application are shown in Appendix B.

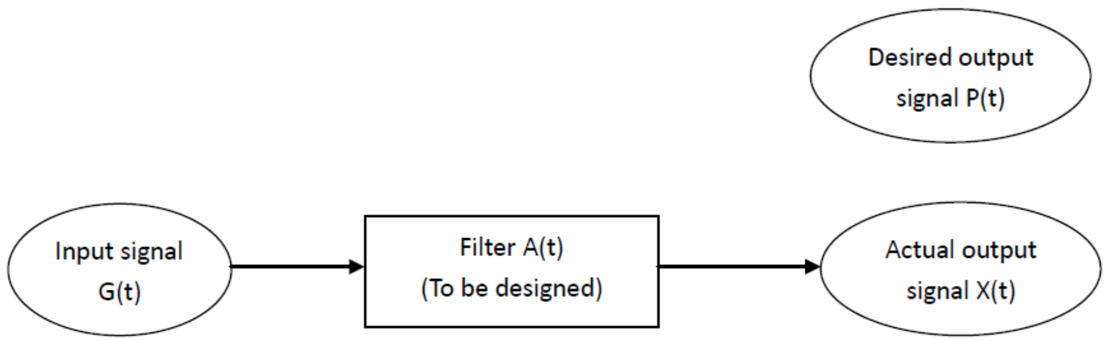

Fig. 4.2: *Wiener filter method*

4.2.2 Spectral division method

4.2.2.1 Theory

Spectral division method for wavelet estimation comes closely from the relationship of P_0 and G_0 in the frequency domain, which is

$$P_0(\vec{r}, \vec{r_s}, \omega) = G_0(\vec{r}, \vec{r_s}, \omega) A(\omega).$$

So that

$$A(\omega) = \frac{P_0(\vec{r}, \vec{r_s}, \omega)}{G_0(\vec{r}, \vec{r_s}, \omega)}. \tag{4.32}$$

While in practice, for avoiding the instability issue that may caused by the division by a zero, we put a small ϵ in the denominator,

$$A(\omega) = \frac{P_0\left(\vec{r}, \vec{r_s}, \omega\right) G_0{}^*(\vec{r}, \vec{r_s}, \omega)}{G_0(\vec{r}, \vec{r_s}, \omega) G_0{}^*(\vec{r}, \vec{r_s}, \omega) + \varepsilon}, \tag{4.33}$$

where $G_0^*(\vec{r}, \vec{r_s}, \omega)$ means the conjugate of $G_0(\vec{r}, \vec{r_s}, \omega)$.

In the test using data set with noise, the results show that the choice of the value of ϵ will affect the prediction of source wavelet.

4.2.2.2 *Relationship of Wiener filter method and spectral division method*

The relationship of recorded data P_0, G_0, and A in the time domain is

$$P_0(t) = A(t) * G_0(t), \tag{4.34}$$

where $*$ means convolution. Now I will show that starting from the above convolution and utilizing the definition of correlation, it is possible to get the equations that the Wiener filter method uses.

First we correlate the trace $P_0(t)$ with Green's function. According to the definition of correlation in the integral form,

$$\begin{aligned}
\phi_{PG}(t) &= \int_{-\infty}^{\infty} P_0(\tau + t) G_0(\tau) d\tau &(4.35)\\
&= \int_{-\infty}^{\infty} P_0(\tau) G_0(\tau - t) d\tau &(4.36)\\
&= \int_{-\infty}^{\infty} P_0(\tau) G_0[-(t - \tau)] d\tau &(4.37)\\
&= P_0(t) * G_0(-t) &(4.38)
\end{aligned}$$

Now plug Equation 4.34 into the above equation, we have

$$\begin{aligned}
\phi_{PG}(t) &= (A(t) * G_0(t)) * G_0(-t) && (4.39)\\
&= A(t) * (G_0(t) * G_0(-t)) && (4.40)\\
&= A(t) * \phi_{GG}(t) && (4.41)\\
&= \int_{-\infty}^{\infty} A(\tau)\phi_{GG}(t-\tau)d\tau && (4.42)
\end{aligned}$$

Comparing with Equation 4.30, which says,

$$\sum_{s=0}^{m} A_s \cdot \phi_{GG}(i-s) = \phi_{PG}(i) \qquad i = 0, 1, 2, ..., m \tag{4.43}$$

we can see that these two equations are eventually the same. One is in a discrete form, and the other is in a continuous form.

4.2.3 Green's theorem

The Green's theorem based wavelet estimation method follows the theory of separating the reference wave P_0 introduced in Chapter 2. The source wavelet $A(\omega)$ can be estimated by

$$A(\omega) = \frac{P_0(\vec{r}, \vec{r_s}, \omega)}{G_0(\vec{r}, \vec{r_s}, \omega)} = \frac{\int_{m.s.} \left[P(\vec{r'}, \omega)\nabla' G_0(\vec{r}, \vec{r'}, \omega) - G(\vec{r}, \vec{r'}, \omega)\nabla' P(\vec{r'}, \omega)\right] \cdot \hat{n} d\vec{r'}}{G_0(\vec{r}, \vec{r_s}, \omega)}. \tag{4.44}$$

The inputs are the measured total wavefield P and its normal derivative ∇P on the measurement surface, rather than the reference wave P_0, which is required by the previous two methods. The Green's theorem method can extract the source signature or radiation pattern, with the inclusion of instrument response of the measuring device. In addition, the integral over the measurement surface can smooth noises in the data. While the other two methods, the Wiener filter method and the spectral division method, both estimate the source wavelet trace by trace. This means they cannot accommodate noisy data very well.

4.3 Test results

In this section, I will compare the three wavelet estimation methods using both synthetic data and field data set.

4.3.1 Synthetic data

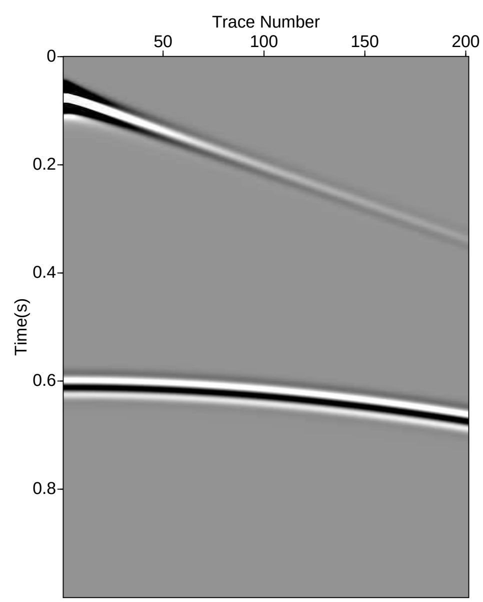

Fig. 4.3: *Synthetic data generated using Cagniard-de Hoop method. P_0 and P_s are not interfering. No noise is included.*

The synthetic data set is generated by Cagniard-de Hoop method, with a 2D line source and 1D subsurface. The source is placed at depth 2 m, and receivers at depth 6 m. The reflector is at 400 m. An example of the data is shown in Figure 4.3, with offset from 0 to 400 m. I purposely generate the data with non-interfering reference wave P_0 and scattered wave P_s, so that P_0 can be extracted directly from the data.

4.3.1.1 Without noises

In the first test, I use perfect data without any noise to test the three wavelet estimation methods.

For the Wiener-filter method and the spectral division method, the reference wave P_0 comes from the data directly, which are shown in Figure 4.3. The estimated wavelet results by using these two methods are shown in Figure 4.4 and Figure 4.5, respectively. The red lines are the true wavelet used in the data modeling, and the green lines are the predicted wavelet. For both of the results, the red line and green line are almost overlapping. The conclusion is that when there is no noise in the data, these two methods can both predict perfect wavelet results very well.

When estimating the wavelet using Green's theorem, we need to use over/under cable to calculate dP/dz. First, I estimate P_0 at depth 18 m (below the cable), then predict the wavelet $A(t)$ result at different offsets. Figure 4.6 shows the predicted wavelet result (green line) and the comparison with the true wavelet (red line). These two lines are also almost overlapping together, indicating the estimated wavelet is accurate.

From the comparison, it is clear that all these three methods can extract the wavelet very well when there is no noise in the data. The Wiener filter method and spectral division method use the reference wave directly, whereas the Green's theorem method uses the total wavefield and its normal derivatives as the inputs. The first two methods

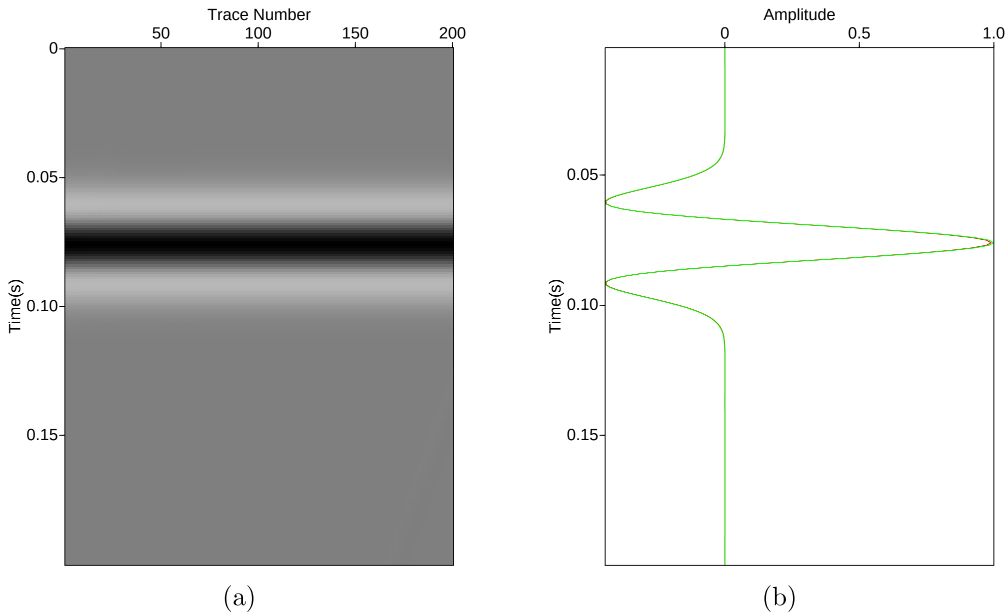

Fig. 4.4: *Wavelet estimation result using Wiener filter method. (a) Wavelet estimated at different offset. (b) Comparison of the true wavelet used in the modeling (red line) and the estimated wavelet (green line).*

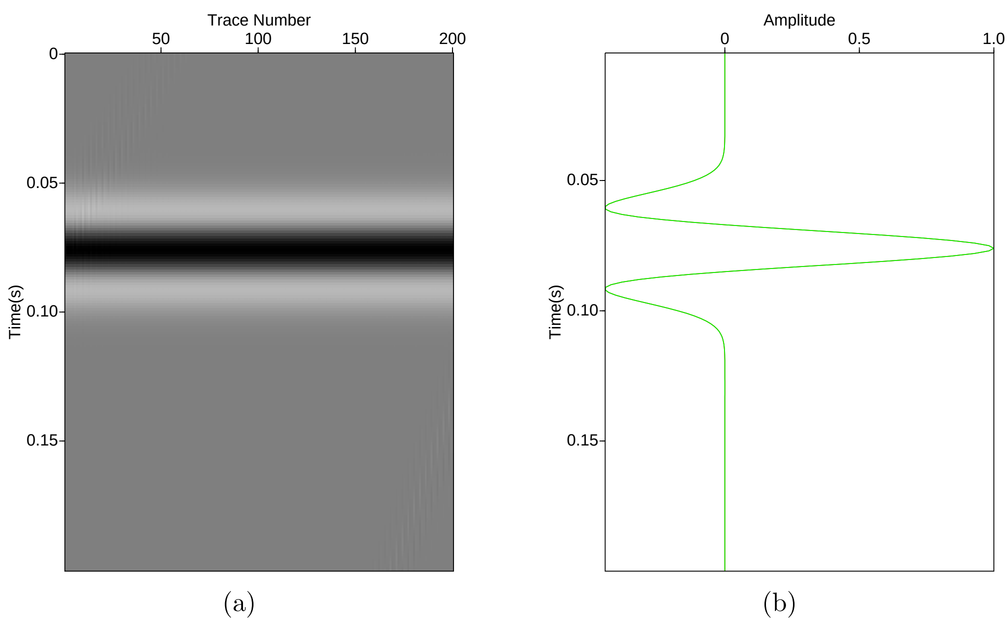

Fig. 4.5: *Wavelet estimation result using spectral division method. (a) Wavelet estimated at different offset. (b) Comparison of the true wavelet used in the modeling (red line) and the estimated wavelet (green line).*

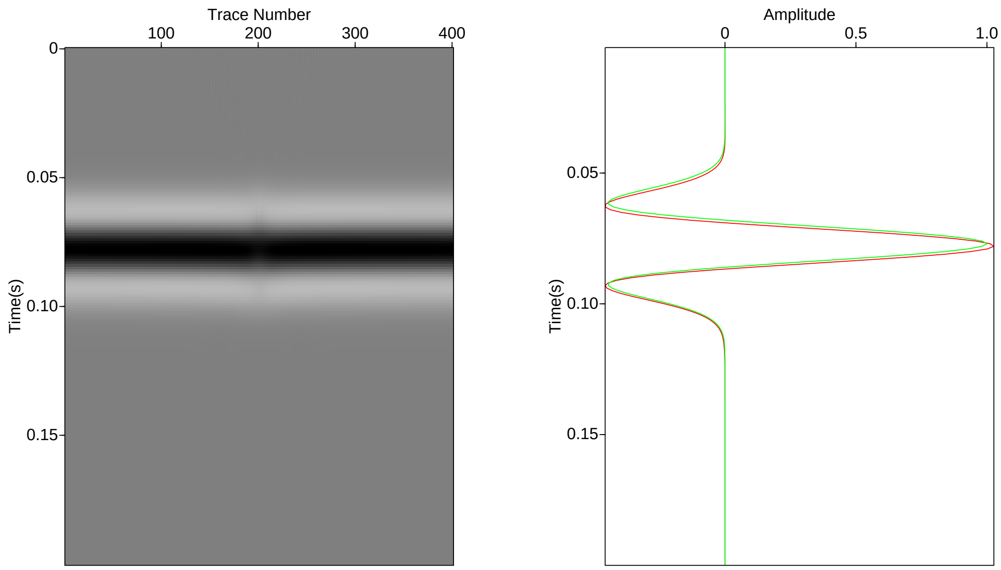

(a) (b)

Fig. 4.6: *Wavelet estimation result using Green's theorem. (a) Wavelet estimated at different offset. (b) Comparison of the true wavelet used in the modeling (red line) and the estimated wavelet (green line).*

are direct and easy to operate. However, in practice, the reference wave may interfere with the scattered wave (e.g., in shallow water area), thus they are not directly available for us to use. In this occasion, the Green's theorem method can serve as a good way to estimate the wavelet.

4.3.1.2 With noise

In the next test, I add a random white noise into the data set in Figure 4.3. In the original data set, as the offset gets larger, the amplitude of P_0 becomes smaller. Therefore, the signal-noise-ratio in the noisy data set is varying throughout the offsets. The data with random noise is shown in Figure 4.7. In order to show the different signal-noise-ratio, I focused in four regions indicated by the number 1,2,3,4.

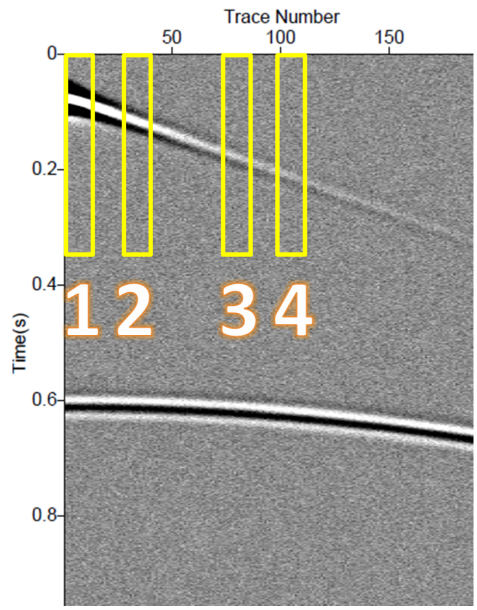

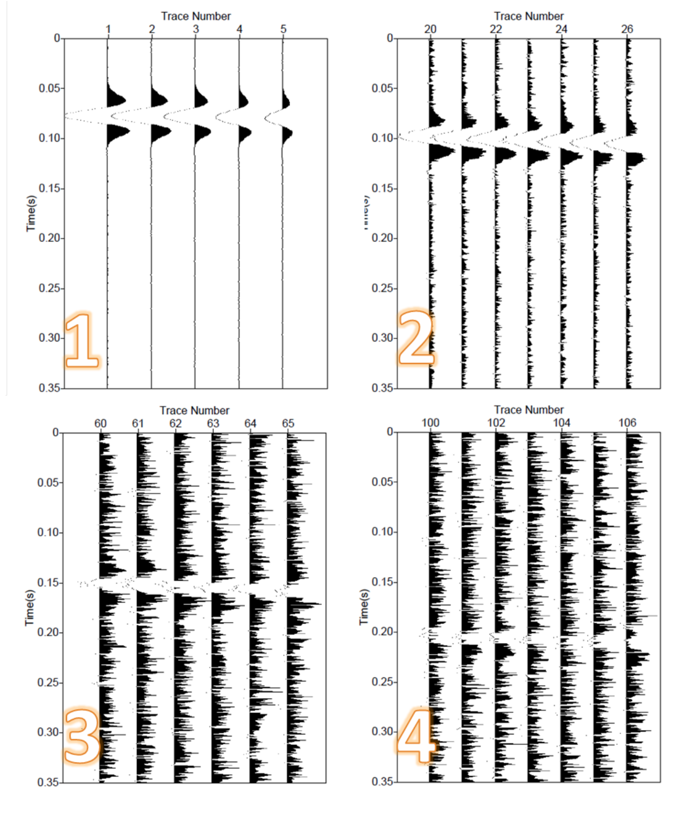

Fig. 4.7: *Synthetic data generated with random white noises. Each number indicates a region with different signal-noise-ratio. The wiggle plots are extracted from the above data set, at four regions indicated by the numbers correspondingly.*

Next, I estimate the source wavelet using these three methods:

(1) The wavelet results performed by using the Wiener filter method is shown in Figure 4.8, correspondingly. When the signal-ratio is large in the near offset region, this method can predict a satisfying wavelet result. However, in the larger noise regions, this method fails to predict a Ricker wavelet shape, which is the true wavelet we used in data modeling.

As Equation 4.30 shows, when using the Wiener filter method, the length of the filter (estimated wavelet) can be decided by us. In the result shown in Figure 4.8, the length of the wavelet is chosen as 301 points (*i.e.*, $m = 301$ in Equation 4.30). The choice of this number will affect the estimated result. Figure 4.9 compares the results when using different lengths of the wavelet. In this particular test, setting the length of the wavelet shorter (301 points vs 501 points) gives a better and stable prediction. This comparison shows that choosing a proper length of the filter can optimize the prediction result.

(2) The wavelet results performed by using the spectral division method is shown in Figure 4.10. Similarly, in the small-noise region, this method can predict the wavelet shape very well, whereas when the noise gets larger compared with the signal, the estimated wavelet becomes more unstable.

In the theory of spectral division method, a small number ϵ is employed for avoiding a division by zero. The test results also indicate that the choice of this small number will affect the estimated result. Figure 4.11 shows the comparison of using different ϵ in this particular test. In Figure 4.10, $\epsilon = 0.0001$ is used for optimizing the wavelet result.

(3) When using the Green's-theorem method, it will first predict the reference wave

P_0 from the total wavefields. P_0 is shown in Figure 4.12. We can see that the noise in the original data set is clearly reduced in the estimated reference wave. Figure 4.13 shows the wavelet estimation at the four different areas. Comparing with the above two methods, Green's theorem demonstrates a more stable and clean result. It can smooth the noise in the data, because the surface integral in the algorithm can cancel the random noise. On the other hand, the Wiener-filter method and the spectral division method both perform wavelet estimation trace by trace, thus they cannot accommodate the noises very well.

In order to compare the results from these three method more clearly, Figure 4.14 and Figure 4.15 put the estimated wavelet results together, showing the three results for both large and small SNR data sets. When the noise is small, these three methods can predict the wavelet correctly. As for a large noise data set, the Wiener filter method and spectral division are less effective as the Green's-theorem method, since the Green's-theorem method utilizes an integral along all the traces, while the other two methods estimate the wavelet trace by trace.

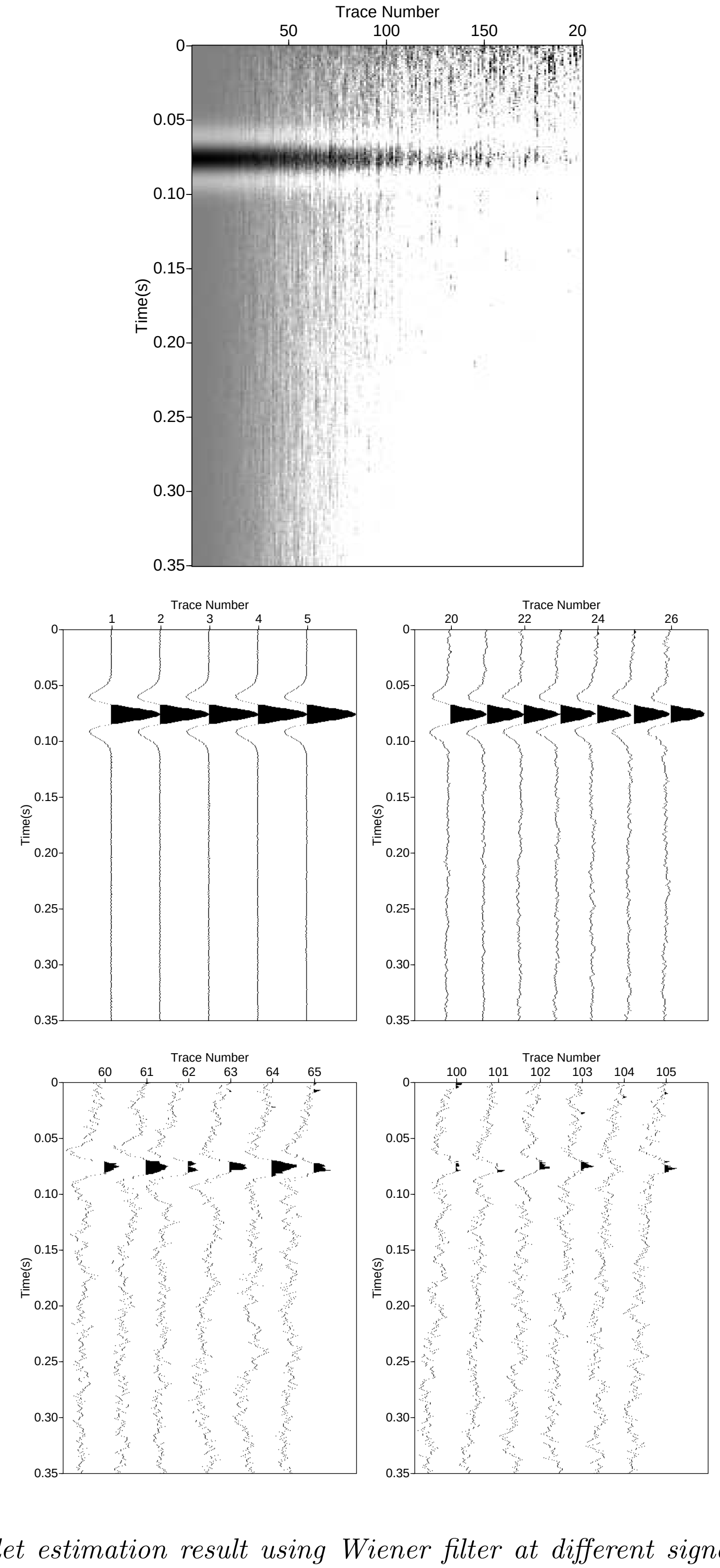

Fig. 4.8: *Wavelet estimation result using Wiener filter at different signal-noise-ratio regions.*

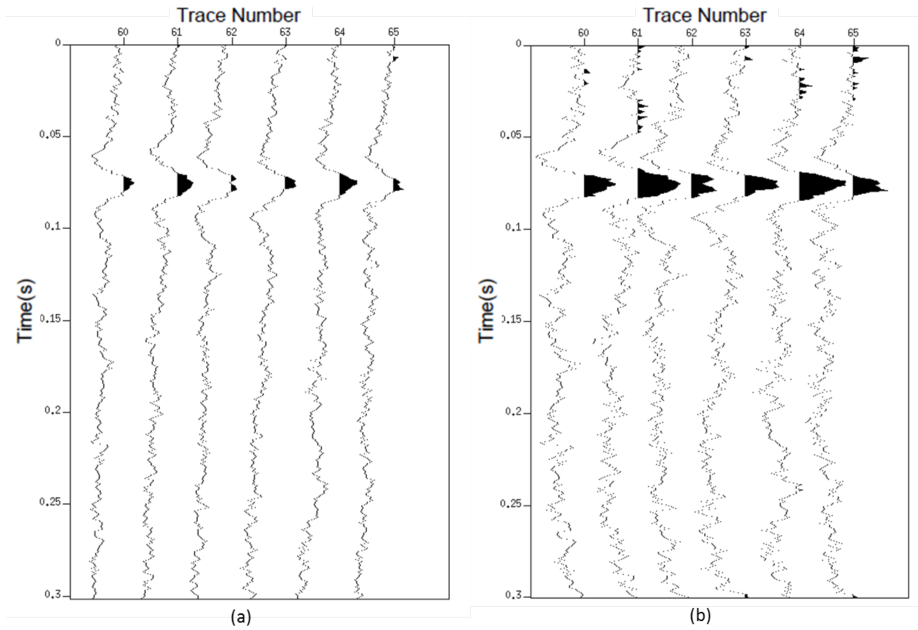

Fig. 4.9: *Estimated wavelet results at region 3 when choosing the length of the wavelet as (a) 501 points and (b) 301 points.*

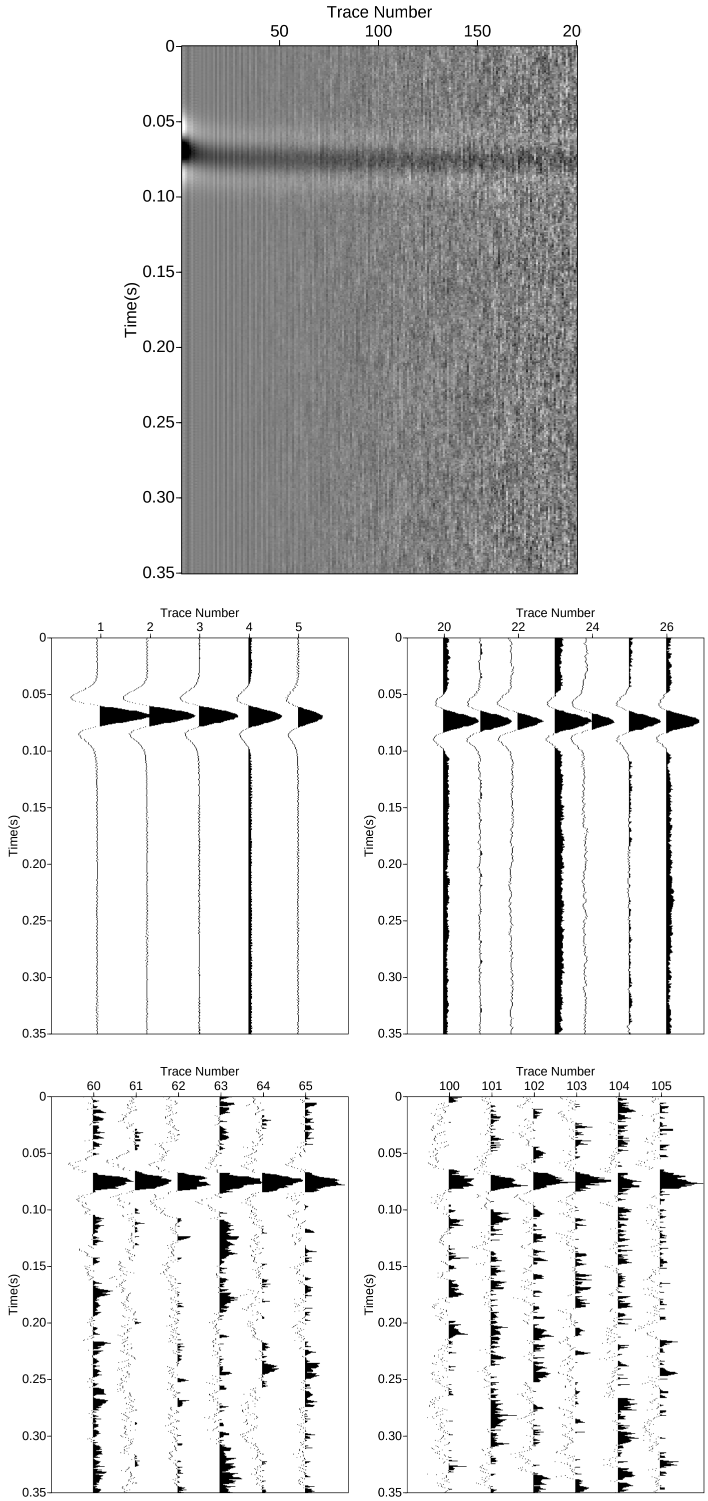

Fig. 4.10: *Wavelet estimation result using spectral division at different signal-noise-ratio regions.*

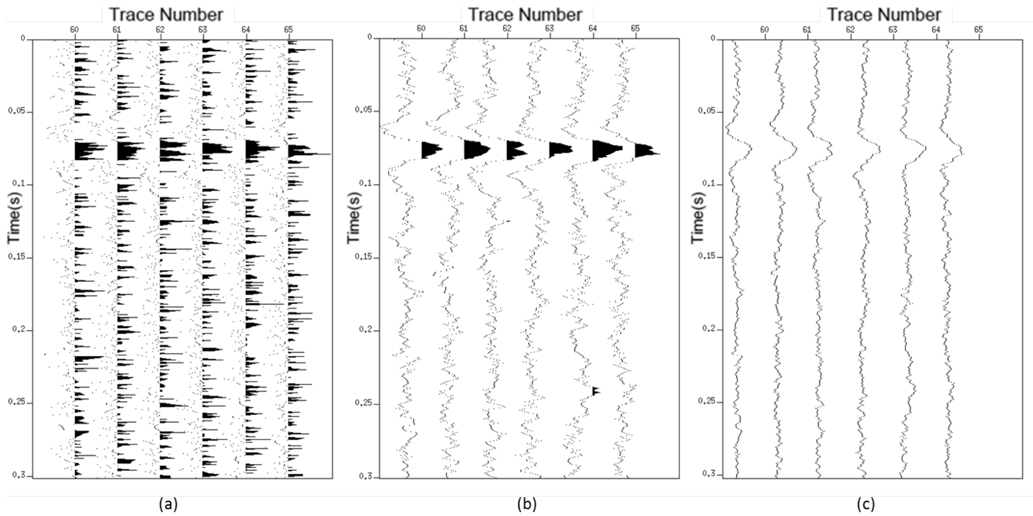

Fig. 4.11: *Estimated wavelet results at region 3 when choosing different ϵ (a) $\epsilon = 0.01$, (b) $\epsilon = 0.0001$, and (c) $\epsilon = 0.00001$.*

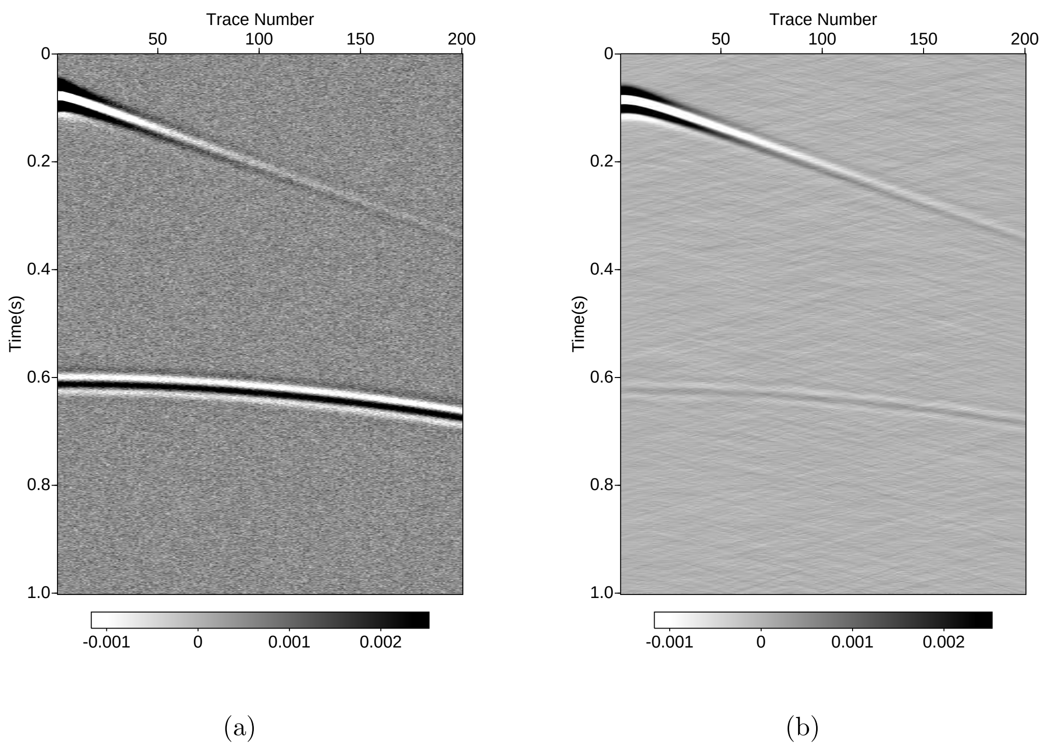

Fig. 4.12: *(a)Input data with noise, (b) the output P_0 using Green's theorem*

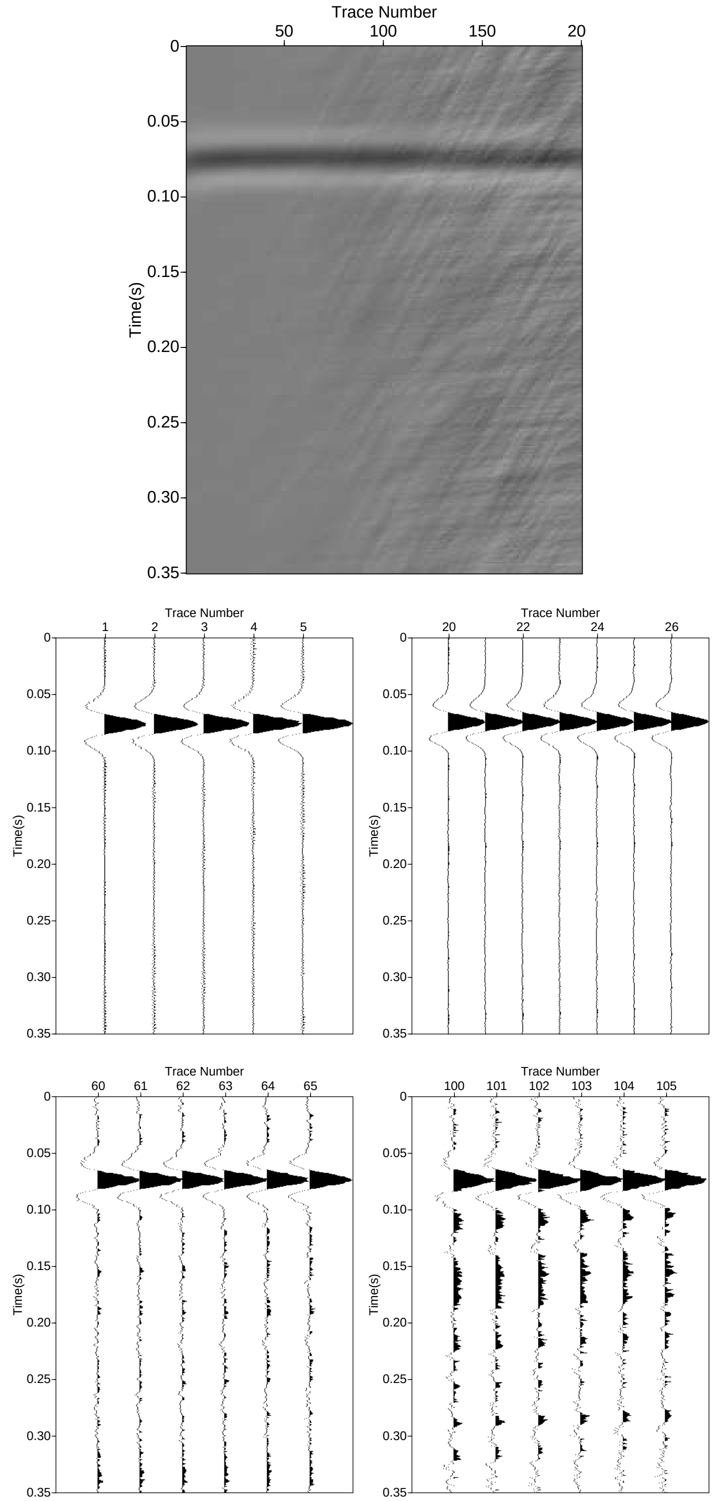

Fig. 4.13: *Wavelet estimation result using Green's theorem at different signal-noise-ratio regions.*

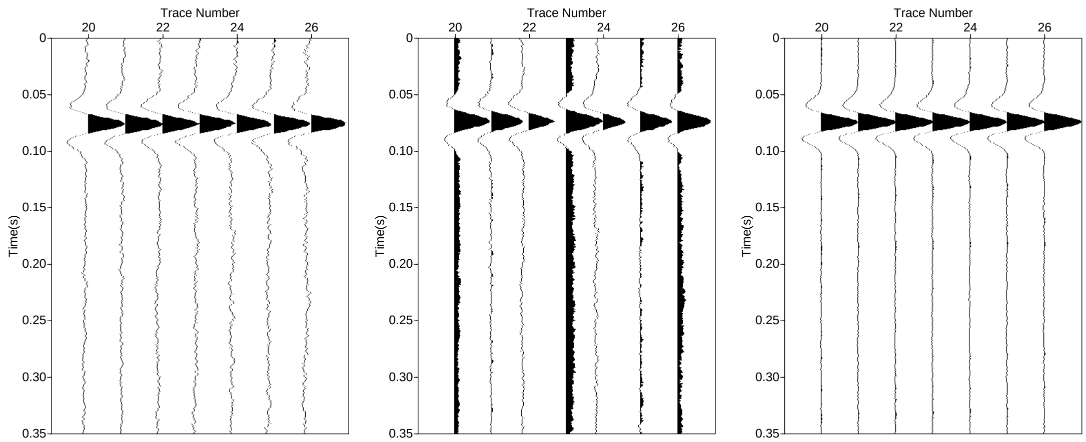

(a) (b) (c)

Fig. 4.14: *Estimated wavelet result when SNR is large using (a) Wiener filter (b) spectral division (c) Green's theorem*

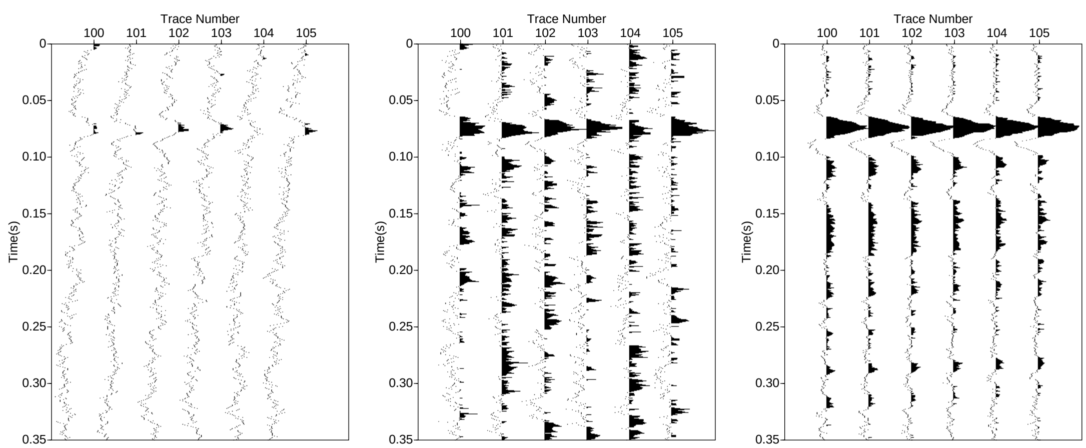

(a) (b) (c)

Fig. 4.15: *Estimated wavelet result when SNR is small using (a) Wiener filter (b) spectral division (c) Green's theorem*

4.3.2 Kristin field data

Kristin field data set is measured at the North Norwegian Sea, and it is the first field data test of ISS depth imaging algorithm (Liu *et al.*, 2011; Weglein *et al.*, 2012a,b). In the depth imaging test, the source wavelet information is essential for regularizing the data, in order to have more low frequency contents, which is required by the ISS imaging algorithm. For this data set, I use the Wiener-filter method to extract the source wavelet from the reference wave and the reference Green's function.

In Kristin data, the reference wave P_0 can be identified from the raw data directly where P_0 and scattered wave P_s do not overlap, as shown in Figure 4.16. The causal

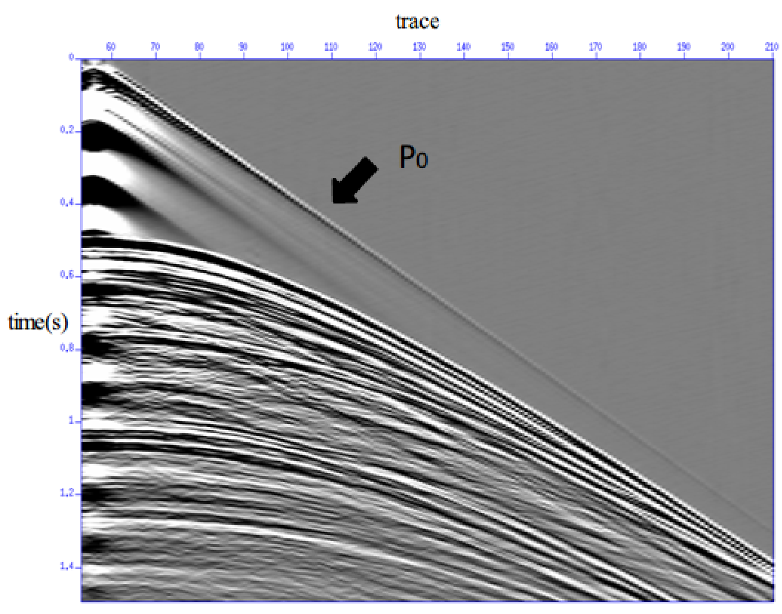

Fig. 4.16: *Kristin data, Type I, cable II (sources at depth 7 m and receivers at depth 18 m)*

reference Green's function is,

$$
\begin{aligned}
G_0(\vec{r}, \vec{r}', \omega) &= \frac{1}{4\pi}\left(\frac{e^{ikR}}{R} - \frac{e^{ikR_I}}{R_I}\right) && (4.45)\\
&= G_0^d + G_0^{FS}, && (4.46)
\end{aligned}
$$

where $k = \omega/c_0$, $\vec{r} = (x, y, z)$, $\vec{r}' = (x', y', z')$ and

$$
\begin{aligned}
R &= \sqrt{(x-x')^2 + (y-y')^2 + (z-z')^2} && (4.47)\\
R_I &= \sqrt{(x-x')^2 + (y-y')^2 + (z+z')^2}. && (4.48)
\end{aligned}
$$

Here G_0^d represents the portion of the direct arrival from the source to the receiver, and G_0^{FS} represents the wave that experiences a reflection at the air-water interface in the reference medium. The only information required for calculating Green's function is the location of the source and receiver, therefore the reference Green's function can be calculated directly.

Having the reference wave P_0 obtained directly from the raw data, the reference Green's function G_0 calculated from the configuration of source and receiver, and using Equation 4.9, the wavelet $A(t)$ can be extracted independently from each trace. In Kristin data cable II with sources located at depth 7 m and receivers at depth 18 m, the wavelet estimation result is shown in Figure 4.17. For cable III (sources at depth 7 m, receivers at depth 25 m), wavelet result is shown in Figure 4.18.

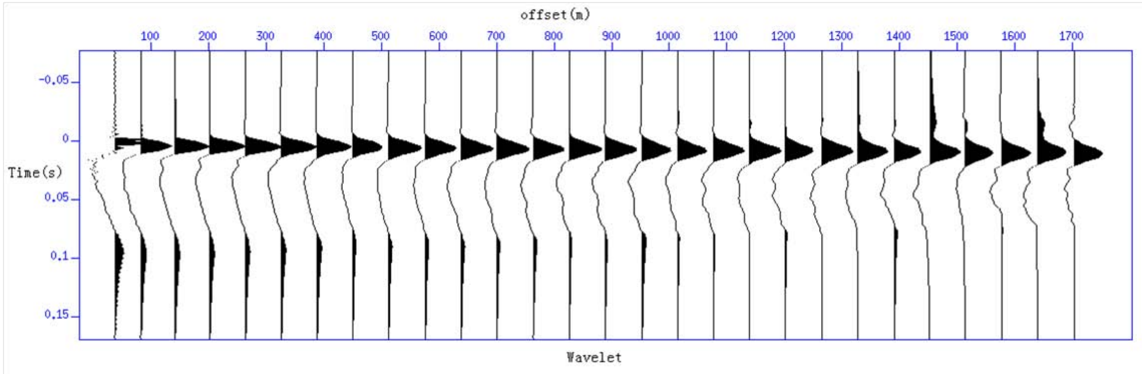

Fig. 4.17: *Wavelet $A(t)$ using Wiener filter method, cable II (sources at depth 7 m and receivers at depth 18 m)*

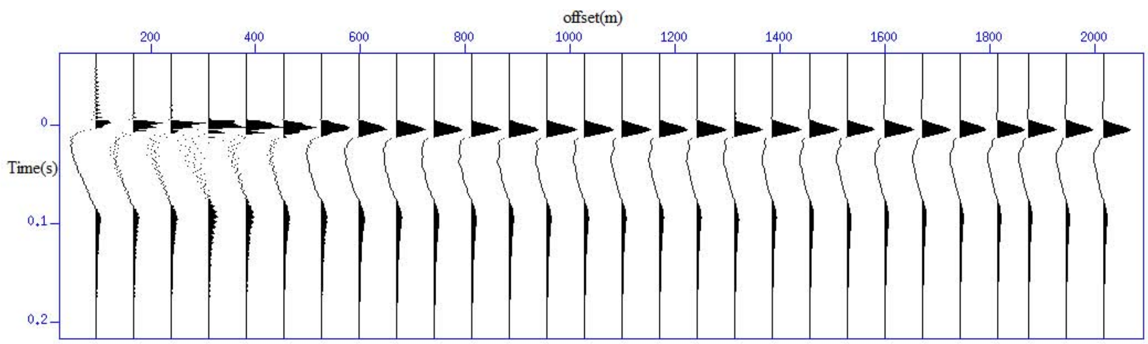

Fig. 4.18: *Wavelet $A(t)$ using Wiener filter method, cable III (sources at depth 7 m and receivers at depth 25 m)*

Discussion The results shown so far are obtained using the total Green's function G_0 for a homogeneous half space of water, which is composed of a direct Green's function G_0^d plus a free surface Green's function G_0^{FS}. If the direct Green's function G_0^d is used instead of the total Green's function G_0 in Equation 4.46, the result is shown in Figure 4.19.

The result in Figure 4.19 can be interpreted as an estimation of the effect of the source in the presence of a free-surface, as proven by the decreasing amplitude trends for increasing offsets. The reason can be found in the expression of G_0^d. As

$$G_0^d(\vec{r}, \vec{r'}, \omega) = \frac{1}{4\pi}\frac{e^{ikR}}{R} \tag{4.49}$$

and

$$G_0(\vec{r}, \vec{r'}, \omega) = \frac{1}{4\pi}(\frac{e^{ikR}}{R} - \frac{e^{ikR_I}}{R_I}), \tag{4.50}$$

at large offset, the two terms of total G_0 tend to cancel each other, thus G_0 gets smaller, whereas G_0^d still gets larger as distance grows. On the other hand, the reference wave P_0 also consists of the direct arrive and its free surface ghost, which will cancel each other at the large offset, too. Therefore, when using the total G_0, the amplitude of wavelet is stable, while G_0^d makes wavelet vanish.

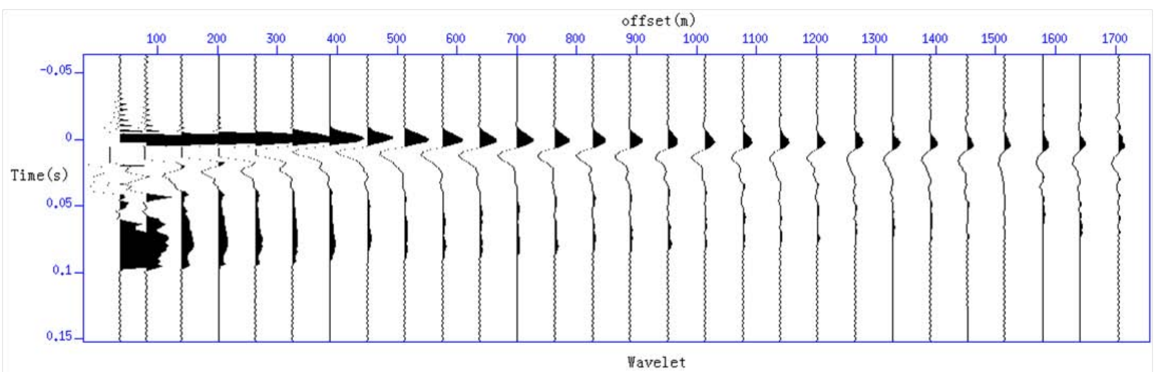

Fig. 4.19: *Wavelet $A(t)$, cable II (sources at depth 7 m and receivers at depth 18 m), using direct Green's function G_0^d.*

4.4 Conclusions

In this chapter, I study and analyze three different source wavelet estimation methods, which are (1) the Wiener-filter method, (2) the spectral division method and (3) the Green's theorem method. In the synthetic data tests, if the data contains no noise, all the three methods can estimate the source signature very well. When the data contains random noise, the Green's theorem method demonstrates strength in smoothing the noises in the results. Because Green's theorem uses a surface integral along all the traces in the data, whereas the other two methods estimate wavelet trace by trace. In the marine field data test, I use Wiener filter method to extract the wavelet from the reference wave directly. The estimated result is utilized in the first ISS depth imaging field test for data regularization purpose.

5. SUMMARY

This dissertation focuses on solving several practical issues in satisfying the prerequisites of ISS multiple removal algorithm. The better the prerequisites are satisfied, the better delivery of the ISS multiple prediction results we can get. In order to satisfy the prerequisites better, more realistic descriptions of the seismic experiment need to be included in the realization of the theories.

For better separating the reference wave from the reflected seismic data, I consider to incorporate the data acquisition design into the data processing. I have shown that for an over/under cable acquisition, there are several practical issues that will affect the wave separation results. Firstly, the depth difference between the over/under cable will affect the wave separation result. The closer of the two cables are, the more accurate prediction results the theory will predict. It is due to the fact that, with a closer over/under cable, the normal derivative of the wavefield on the measurement surface becomes more accurate, under a finite difference approximation. Secondly, the choice of the prediction point also influences the separation results. The form of the Green's function in the (x, ω) domain restricts us from predicting the separated wave on the cable. The prediction points cannot be chosen on the cable, but at least half of the receiver sampling away from the cable. By converting Green's theorem to the wavenumber domain, it becomes possible to predict the reference wave/scattered wave on the cable, which means, isolate them from the measured data. The same issue is also being observed in the application of Green's theorem for deghosting.

Chapter 4 starts to address an issue when extending the prerequisites satisfaction to the on-shore exploration. The near surface medium property on land is often complex and difficult to determine. ISS methods require that the reference medium agree with the actual medium at and above the measurement surface. Thus, determining the reference medium property becomes a big challenge for land application. I propose to use invariances of the source wavelet estimation as the criteria for obtaining the correct reference velocity. This idea is illustrated and tested using a marine environment. For data generated from a point source, the invariance happens at every point below the measurement surface, and for data with radiation pattern, the invariance can be found along one radiation angle. In the future study, the similar thinking of using the invariances in the reference wave prediction could be use, to move towards complex on-shore or ocean bottom reference medium problems.

The source signature information is essential in many seismic data processing steps, including multiple removal and depth imaging. In Chapter 3, I study three different wavelet estimation methods: (1) the Wiener filter method, (2) the spectral division method and (3) the Green's theorem method. Each method has its own advantages and disadvantages. The Wiener filter method and spectral division method offer a direct way of extracting wavelet from the reference wave, but the reference wave may not always be available from the data. Synthetic data with noise results show that the Green's theorem method can smooth the noise in the data very well, because it contains a surface integral along all the traces, whereas the other two methods only perform wavelet estimation trace by trace. The Kristin field data test using Wiener filter method provides a useful source wavelet information for the data regularization in the first ISS depth imaging field data test.

REFERENCES

ARAÚJO, F. V. 1994. Linear and non-linear methods derived from scattering theory: backscattered tomography and internal multiple attenuation. Ph.D. thesis, Universidade Federal da Bahia.

CARLSON, D., SLLNER, W., TABTI, H., BROX, E., AND WIDMAIER, M. 2007. Increased resolution of seismic data from a dualsensor streamer cable. *SEG Technical Program Expanded Abstracts*, 994–998.

CARVALHO, P. M. 1992. Free-surface multiple reflection elimination method based on nonlinear inversion of seismic data. Ph.D. thesis, Universidade Federal da Bahia.

FERREIRA, A. 2011. Internal multiple removal offshore brazil seismic data using the inverse scattering series. M.S. thesis, University of Houston.

FU, Q., LUO, Y., KELAMIS, P. G., HUO, S., SINDI, G., HSU, S.-Y., AND WEGLEIN, A. B. 2010. The inverse scattering series approach towards the elimination of land internal multiples. *SEG Technical Program Expanded Abstracts*, 34563461.

HERRERA, W. AND WEGLEIN, A. B. 2013. Eliminating first-order internal multiples with downward reflection at the shallowest interface: Theory and initial examples. *SEG Technical Program Expanded Abstracts*, 4131–4135.

Liang, H., Ma, C., and Weglein, A. 2013. General theory for accommodating primaries and multiples in internal multiple algorithm: analysis and numerical tests.. *SEG Technical Program Expanded Abstracts*, 4178–4183.

Liu, F., Li, X., and Weglein, A. B. 2011. Addressing innate data limitations in iss imaging algorithms: distinct data regularization methods to address different types of data limitations, to facilitate and allow specific iss imaging steps and goals. *2010 M-OSRP Annual Report*, 50–81.

Loveridge, M., Parks, G., Hatton, L., and Worthington, M. 1984. Effects of marine source array directivity on seismic data and source signature deconvlution. *First Break 2,* 7, 16–22.

Ma, C., Liang, H., and Weglein, A. B. 2011. Modifying the leading order iss attenuator of first-order internal multiples to accommodate primaries and internal multiples: fundamental concept and theory, development, and examples exemplified when three reflectors generate the data. *2010 M-OSRP Annual Report*, 133147.

Mayhan, J., Terenghi, P., Weglein, A. B., and Chemingui, N. 2011. Green's theorem derived methods for preprocessing seismic data when the pressure p and its normal derivative are measured. *SEG Technical Program Expanded Abstracts*, 2722–2726.

Mayhan, J. and Weglein, A. B. 2013. First application of green's theorem-derived source and receiver deghosting on deep-water gulf of mexico synthetic (seam) and field data. *Geophysics 78*, WA77–WA89.

Moldoveanu, N., Combee, L., Egan, M., Hampson, G., Sydora, L., and Abriel, W. 2007. Over/under towed-streamer acquisition: A method to extend seismic bandwidth to both higher and lower frequencies. *The Leading Edge Jan*, 41–58.

Morse, P. M. and Feshbach, H. 1953. *Methods of theoretical physics*. McGraw-Hill Book Co.

Robinson, E. A. and Treitel, S. 1980. *Geophysical signal analysis*. Englewood Cliffs, N.J.Prentice-Hall.

Sheriff, R. E. and Geldart, L. P. 1994. *Exploration Seismology*. Vol. 2nd ed. Cambridge; New York: Cambridge University Press.

Tang, L., Mayhan, J., Yang, J., and Weglein, A. B. 2013. Using green's theorem to satisfy data requirements of multiple removal methods: The impact of acquisition design. *SEG Technical Program Expanded Abstracts*, 4392–4396.

Taylor, J. R. 1972. *Scattering theory: the quantum theory of nonrelativistic collisions*. John Wiley & Sons, Inc.

Vaseghi, S. V. 2008. *Advanced digital signal processing and noise reduction*, 4th ed. Chichester, U.K. : J. Wiley Sons, 2008.

Weglein, A. B. 2013. The multiple attenuation toolbox: Progress, challenges and open issues. *SEG Technical Program Expanded Abstracts*, 4493–4499.

Weglein, A. B., Araújo, F. V., Carvalho, P. M., Stolt, R. H., Matson, K. H., Coates, R. T., Corrigan, D., Foster, D. J., Shaw, S. A., and Zhang, H. 2003. Inverse scattering series and seismic exploration. *Inverse Problems* 19, R27–R83.

WEGLEIN, A. B., GASPAROTTO, F. A., CARVALHO, P. M., AND STOLT, R. H. 1997. An inverse-scattering series method for attenuating multiples in seismic reflection data. *Geophysics 62,* 6 (November-December), 1975–1989.

WEGLEIN, A. B., LIANG, H., WU, J., MAYHAN, J. D., TANG, L., AND AMUNDSEN, L. 2013. A new greens theorem de-ghosting method that simultaneously: (1) avoids a finite difference approximation for the normal derivative of the pressure and, (2) avoids the need for replacing the normal derivative of pressure with the vertical component of particle velocity, thereby avoiding issues that can arise within each of those two assumptions/approaches: Theory and analytic and numeric examples. *Journal of Seismic Exploration 22*, 413–426.

WEGLEIN, A. B., LIU, F., LI, X., TERENGHI, P., KRAGH, E., MAYHAN, J., WANG, Z., MISPEL, J., AMUNDSEN, L., LIANG, H., TANG, L., AND HSU, S. 2012a. First field data examples of inverse scattering series direct depth imaging without the velocity model. *SEG Technical Program Expanded Abstracts*, 1–6.

WEGLEIN, A. B., LIU, F., LI, X., TERENGHI, P., KRAGH, E., MAYHAN, J., WANG, Z., MISPEL, J., AMUNDSEN, L., LIANG, H., TANG, L., AND HSU, S. 2012b. Inverse scattering series direct depth imaging without the velocity model: First field data examples. *Journal of Seismic Exploration 21,* 1, 1–28.

WEGLEIN, A. B., MAYHAN, J. D., AMUNDSEN, L., LIANG, H., WU, J., TANG, L., LUO, Y., AND FU, Q. 2013. Greens theorem de-ghosting algorithms in k, (e.g., de-ghosting) as a special case of x, algorithms (based on greens theorem) with: (1) significant practical advantages and disadvantages of algorithms in each domain, and (2) a new message, implication and opportunity for marine towed streamer, ocean bottom and on-shore acquisition and applications. *Journal of Seismic Exploration 22*, 289412.

Weglein, A. B. and Stolt, R. 2014. *Seismic Imaging and Inversion II.* Cambridge University Press. In press.

Wiener, N. 1949. *Extrapolation, interpolation, and smoothing of stationary time series : with engineering applications.* Cambridge, MA : Technology Press of the Massachusetts Institute of Technology.

Yang, J., Mayhan, J., Tang, L., and Weglein, A. B. 2013. Accommodating the source (and receiver) array in free-surface multiple elimination algorithm: Impact on interfering or proximal primaries and multiples. *SEG Technical Program Expanded Abstracts*, 4184–4189.

Zhang, J. 2007. Wave theory based data preparation for inverse scattering multiple removal, depth imaging and parameter estimation: analysis and numerical tests of green's theorem deghosting theory. Ph.D. thesis, University of Houston.

Zou, Y. and Weglein, A. B. 2013. A new method to eliminate first order internal multiples for a normal incidence plane wave on a 1d earth. *SEG Technical Program Expanded Abstracts*, 4136–4140.

APPENDICES

A. DERIVATION OF 2D G_0^{DD}

This appendix provides mathematic details on calculation of the Green's function G_0^{DD} which vanishes both on the over and the under cables. In Appendix B in Zhang (2007), a 2D G_0^{DD} is shown, whose values vanish on the free surface ($z = 0$) and on one cable ($z = a$). In this appendix, G_0^{DD} vanishes on two cables at different depth $z = a$ and $z = b$. This Green's function will be used to construct the wavefield and its normal derivatives at a new depth between the two cables, as Equation 2.6 and 2.7 have shown.

Assume that a 2D source is at (ξ, η), and two cables are located at $z = a$ and $z = b$ ($b > a$). The Green's function satisfies the wave equation,

$$(\nabla^2 + k^2)G_0^{DD} = \delta(x - \xi)\delta(z - \eta). \tag{A.1}$$

In order to make $G_0^{DD} = 0$ when $z = a$ and $z = b$, it is reasonable to assume it has this form,

$$G_0^{DD}(x, z; \xi, \eta) = \sqrt{\frac{2}{a}} \sum_{n=1}^{\infty} g_n(x) \sin\left(\frac{\pi n}{b - a}(z - a)\right). \tag{A.2}$$

Now plug Equation A.2 into Equation A.1, the result is,

$$\begin{aligned}
LHS &= \left(\frac{\partial^2}{\partial x^2}+\frac{\partial^2}{\partial z^2}+k^2\right)G_0^{DD}(x,z,\xi,\eta) \\
&= \sqrt{\frac{2}{a}}\sum_{n=1}^{\infty}\left[\frac{d^2}{dx^2}-\frac{n^2\pi^2}{(b-a)^2}+k^2\right]g_n(x)\sin\left(\frac{\pi n}{b-a}(z-a)\right) \\
&= \delta(x-\xi)\delta(z-\eta) = RHS. \qquad \text{(A.3)}
\end{aligned}$$

Now multiply $\sqrt{\frac{2}{a}}\sin\left(\frac{m\pi}{b-a}(z-a)\right)$ on both sides of the equation, and integrating over z from 0 to a, we have,

$$\frac{d^2}{dx^2}g_m(x)-(\frac{m^2\pi^2}{(b-a)^2}-k^2)g_m(x)=\sqrt{\frac{2}{a}}\sin\left(\frac{m\pi}{b-a}(\eta-a)\right)\delta(x-\xi). \qquad \text{(A.4)}$$

When deriving the above equation, we utilized the relationship,

$$\int_0^a \sin\left(\frac{n\pi}{b-a}(z-a)\right)\sin\left(\frac{m\pi}{b-a}(z-a)\right)dz=\frac{a}{2}\delta_{mn}, \qquad \text{(A.5)}$$

when $b < 2a$.

Since the solution should be physical, we assume that $g_m(x)$ has this form,

$$\begin{cases} g_m(x) = Ae^{k_x x} & x < \xi \\ g_m(x) = Be^{-k_x x} & x > \xi \end{cases} \qquad \text{(A.6)}$$

Assuming $k_x^2 = \frac{m^2\pi^2}{(b-a)^2} - k^2 > 0$, when $x = \xi$, the boundary condition gives,

$$\begin{aligned}
k_x A e^{k_x\xi} &= k_x B e^{-k_x\xi} \qquad \text{(A.7)} \\
-Ak_x e^{k_x\xi} - Bk_x e^{-k_x\xi} &= \sqrt{\frac{2}{a}}sin\left(\frac{m\pi}{b-a}(\eta-a)\right) \qquad \text{(A.8)}
\end{aligned}$$

Then A and B can be solved as,

$$A = -\frac{1}{k_x}\frac{1}{\sqrt{2a}} sin\left(\frac{m\pi}{b-a}(\eta-a)\right) e^{-k_x\xi} \quad (A.9)$$

$$B = -\frac{1}{k_x}\frac{1}{\sqrt{2a}} sin\left(\frac{m\pi}{b-a}(\eta-a)\right) e^{k_x\xi} \quad (A.10)$$

So,

$$g_m(x) = -\frac{1}{k_x}\frac{1}{\sqrt{2a}} sin\left(\frac{m\pi}{b-a}(\eta-a)\right) e^{-k_x|x-\xi|}. \quad (A.11)$$

Now we obtain the form of G_0^{DD}, which is,

$$G_0^{DD} = -\frac{1}{a}\sum_{n=1}^{\infty}\frac{1}{sqrt\frac{n^2\pi^2}{(b-a)^2}-k^2} sin\left(\frac{n\pi}{b-a}(\eta-a)\right) e^{-\sqrt{\frac{n^2\pi^2}{(b-a)^2}-k^2}|x-\xi|} sin\left(\frac{n\pi}{b-a}(z-a)\right). \quad (A.12)$$

It is clear that $G_0^{DD} = 0$ when $z = a$ or $z = b$. The assumptions of the above solution are $b < 2a$ and $\frac{n^2\pi^2}{(b-a)^2} - k^2 > 0$, which often can be satisfied.

Differentiate Equation A.12, we can obtain dG_0^{DD}/dz, which is,

$$\frac{d}{dz}G_0^{DD} = -\frac{n\pi}{a(b-a)} \cdot \sum_{n=1}^{\infty}\frac{1}{\sqrt{\frac{n^2\pi^2}{(b-a)^2}-k^2}} sin\left(\frac{n\pi}{b-a}(\eta-a)\right) e^{-\sqrt{\frac{n^2\pi^2}{(b-a)^2}-k^2}|x-\xi|} cos\left(\frac{n\pi}{b-a}(z-a)\right). \quad (A.13)$$

B. DETAILED STEPS IN APPLYING THE WIENER FILTER

From the theory introduced in Section 4.2.1, the specific steps of doing wavelet estimation using the Wiener-filter method are as follows.

1. Prepare reference Green's function (input signal) as discrete series $(G_0, G_1, G_2, ..., G_n)$ with length $n{+}1$ and reference wave (desired signal) as discrete series $(P_0, P_1, P_2, ..., P_{m+n})$ with length $m + n + 1$. Assume the length of filter (wavelet) is $m + 1$. In Kristin data's case, we assume the wavelet has 501 discrete points.

2. Calculate the auto-correlation of input signal $(G_0, G_1, G_2, ..., G_n)$ for lag from 0 to m, i.e.

$$\begin{aligned}
\phi_{GG}(0) &= \sum_{t=0}^{n} G_t \cdot G_t = G_0^2 + G_1^2 + G_2^2 + ... + G_n^2 && \text{(B.1)} \\
\phi_{GG}(1) &= \sum_{t=0}^{n-1} G_t \cdot G_{t+1} = G_0 G_1 + G_1 G_2 + G_2 G_3 + ... G_{n-1} G_n && \text{(B.2)} \\
&\vdots && \text{(B.3)} \\
\phi_{GG}(m) &= \sum_{t=0}^{n-m} G_t \cdot G_{t+1} = G_0 G_m + G_1 G_{m+1} + ... + G_{n-m} G_n && \text{(B.4)}
\end{aligned}$$

3. Calculate the cross-correlation of the desired signal $(P_0, P_1, P_2, ..., P_{m+n})$ and the

input signal $(G_0, G_1, G_2, ..., G_n)$ for lag from 0 to m, i.e.

$$\phi_{PG}(0) = \sum_{t=0}^{n} P_t \cdot G_t = P_0G_0 + P_1G_1 + P_2G_2 + ... + P_nG_n \tag{B.5}$$

$$\phi_{PG}(1) = \sum_{t=0}^{n-1} P_t \cdot G_{t+1} = P_0G_1 + P_1G_2 + P_2G_3 + ...P_{n-1}G_n \tag{B.6}$$

$$\vdots \tag{B.7}$$

$$\phi_{PG}(m) = \sum_{t=0}^{n-m} P_t \cdot G_{t+1} = P_0G_m + P_1G_{m+1} + ... + P_{n-m}G_n \tag{B.8}$$

4. Plug all the ϕ_{GG} and ϕ_{PG} into Equations 4.31. Using Toeplitz recursion, coefficients of filter $(A_0, A_1, A_2, ..., A_m)$ can be solved. In this way the wavelet signature is estimated.